NTNU
Innovation and Creativity

# Numerical Simulation of Interacting Bodies with Delays; Application to Marine Seismic Source Arrays.

**Jens Fredrik Barra Wisløff**

Master of Science in Physics and Mathematics
Submission date: July 2007
Supervisor: Brynjulf Owren, MATH

Norwegian University of Science and Technology
Department of Mathematical Sciences

# Problem Description

In this project we study numerical methods for a certain class of delay differential equations describing the delayed interaction between bodies. In mathematical terms one has a system partitioned into n subsystems such that the kth subsystem interacts with the other n-1 subsystems exclusively through delay terms.
Such differential equations arise in many applications, in particular we shall be concerned with that of airguns configured in an array used for marine seismic exploration. An important issue to consider is the case when the delays are short, meaning that an efficient integrator should use a steplength which is larger than the smallest delay. We will derive schemes which are tailored for such situations, and optimized with respect to accuracy and efficiency. Such methods lead to systems of algebraic equations and as a part of the project we will consider specially designed techniques for handling the linear algebra problems that arise when solving these.
A benchmark for all new schemes derived will be the Kirkwood-Bethe model which describes the dynamics of an oscillating air bubble produced by an airgun.

Assignment given: 05. February 2007
Supervisor: Brynjulf Owren, MATH

# Abstract

This master thesis has looked at numerical simulation of interacting bodies with delays, especially the situation involving interacting airguns in seismic source arrays. The equations describing the airguns have been derived and the interaction between the airguns has been studied. The resulting delay differential equations have been solved with methods that handle step sizes larger than the delays. The accuracy and efficiency of these methods have been investigated, and compared with Matlab solvers.

# Preface

This master thesis is a continuation of my project work on stiffness in the equations describing the motion of an airgun bubble. The subject was first brought to my attention by Brynjulf Owren, professor at NTNU, Department of Mathematical Sciences and my interest in the subject grew as I learned more about it.

The work opportunity given to me by PGS (Petroleum Geo-Services) has encouraged me to continue on some parts of my project work in this master thesis.

I would like to thank my supervisor Brynjulf Owren for competent guidance, Martin Landrø, professor at NTNU, Department of Petroleum Engineering and Applied Geophysics for first hand information about airgun simulations, Lars Eirik Bø, 4th grade at NTNU, Industrial Mathematics for proofreading and psychological support and finally my parents for encouraging words.

# Contents

# 1 Introduction

Nearly 40% of the worlds total energy consumption is provided by oil, and forecasts predict that although greater and greater efforts are put into renewable energy sources, it will stay this way for at least another 25 years [1]. Combined with a steady increase in the worlds total energy consumption, more oil will be needed.

Today, Norway produces oil and gas from reservoirs beneath the ocean floor. These reservoirs are found by seismic surveys which provide an image of the subsurface geological structure. The accuracy of these images is very important because they only give a certain probability for the existence of an oil or gas reservoir. There is a fine line between drilling and not drilling, and the comprehensive costs involved in drilling a well justify a considerable amount of effort in optimizing the subsurface images so drilling empty wells can be avoided.

A seismic survey consists of creating a pressure wave and record its reflection from the subsurface layers. The reflection and refraction of the wave occur at the interfaces between layers with different acoustical properties, and the recording of the reflected wave is done by hydrophones located at the sea surface. The recorded data is analyzed to recreate the subsurface geology. This recreation is an inverse problem without any unique solution and data from series of trials are used to provide the most probable geological composition.

The transmitted pressure wave or signal picks up noise on its way from the source to the hydrophones. To avoid as much of this noise as possible a sharp and precise pressure wave is desired. The ideal signal would be Diracs delta function which of course is impossible to create in practice [10]. The ability to adjust and manipulate the transmitted pressure wave depends on the knowledge of the source. Varying outer conditions affects the behavior of the source, and a strict control of the quality of the transmitted signal is needed.

Today, seismic waves are normally created by airguns. Airguns have proven remarkably stable and produce the same output pressure waveform shot after shot. The airguns can be coupled in clusters normally consisting of two guns, and several clusters are lined up to create an array. The airguns in the array are of different sizes and they are fired with small time delays such that their pressure waves interfere to form a joint sharp and precise wave. This is achieved by constructive interference of the primary peak of the wave, and destructive interference of the following peaks. The settings needed to create the ideal transmitted signal, which depends on outer conditions such as sea depth and temperature, are obtained by numerical simulation. The

Figure 1.1: An airgun on deck.

regularity of the array, e.g. whether the output signal is of acceptable quality if one of the airguns fail, is analyzed by simulations as well.

Ever since the airgun was introduced as a seismic source the physics involved in an airgun blast has been thoroughly studied starting with the work by Ziolkowski in 1970 [11]. A typical airgun consists of two chambers (see figure 1.2). The lower chamber, the firing chamber, gets filled with high pressure air and by release of the shuttle the air finds its way through the ports and creates an oscillating air bubble in the surrounding water. The kinetic entalpi at the bubble wall propagates through the water creating a pressure pulse. The airgun is fired 5-15 meters below the sea surface, has a 100-1000 cubic centimeters chamber and a chamber pressure of 100-300 bar. The pressure wave created has an amplitude of 0.5-10 bar-m.

In a two-gun cluster the pressure wave from one airgun will hit the neighboring airgun, and together with the reflection from the sea surface, called the ghost, it changes the behavior of the gun. Hence, the interaction between the airguns must be included in the physical model. The ghost pressure will also be significant in the far-field where it interferes with the direct pressure wave.

This master thesis is a continuation of my project on the stiffness of

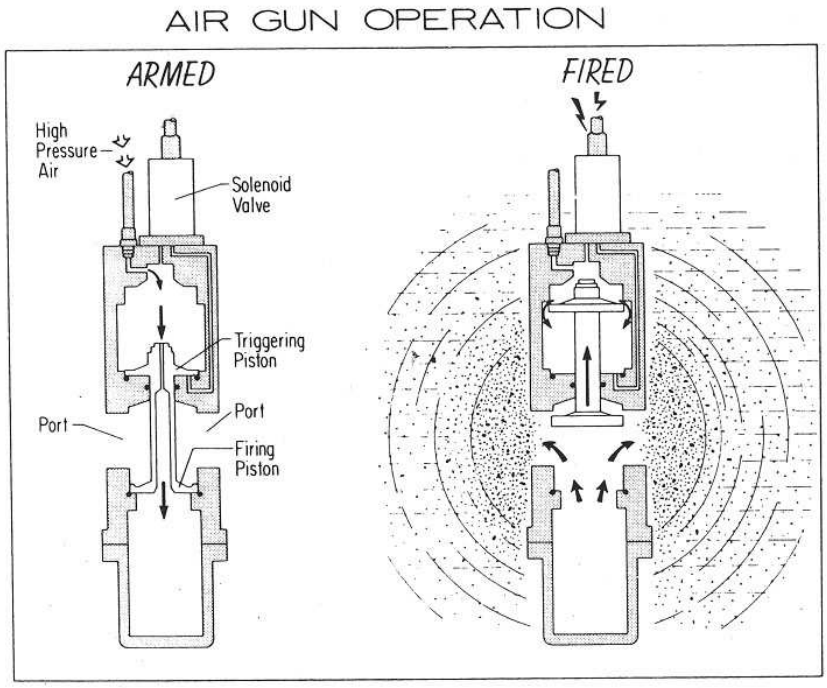


Figure 1.2: Illustration of an air gun blast.

the equations describing one airgun bubble and will proceed to derive the equations describing the motion of the airgun bubble before a more general setting of interacting bodies with delays will be considered. Some problems one may encounter when solving such equations numerically are introduced. The solution to these problems lies in special numerical methods for solving delay differential equations. Simple simulations of both a single airgun and a two-gun cluster will be run. The impact of the interacting pressure waves will be illustrated, and finally the performance of the special numerical methods applied to the airgun equations will be investigated.

# 2 Modeling an airgun bubble

There exist several models which describe the movement of an airgun bubble in water. Different physical assumptions and different simplifications lead to different solutions. The simplest model was first derived by Rayleigh in 1917 [8, Appendix B] and is quite easy to understand (see A.1). A more complicated model is based on the physical observations made by Kirkwood and Bethe in 1942 [7] and applied to bubble dynamics by Ziolkowski in 1970 [11]. Airgun simulations are today based on the Kirkwood-Bethe model with some empirical adjustments.

## 2.1 Kirkwood-Bethe equation

Rayleigh assumes in his model incompressibility of the medium that surrounds the bubble. We need to reject this simplification to handle compressible liquids like water. Kirkwood and Bethe began working with underwater explosions during the second world war. They found that when a charge of TNT blows, not only the first pressure wave from the blast, but also the pressure wave from the oscillating gas bubble created by the chemical reactions is significant for the total transmitted pressure wave. The physics involved is complicated and only an outline of the theory based on Ziolkowski's adaptation will be presented here.

We consider a gas filled cavity in a liquid of infinite extent. The delayed transport of gas from the airgun chamber through the ports and into the surrounding liquid will be included in the model by first releasing only a part of the gas in the chamber and then gradually release the remaining gas with adjustable (but constant) release velocity.

### 2.1.1 Model

We assume spherical symmetry. In other words we neglect the gravity and irregularities as placement of the ports etc. The velocity $\vec{u} = \mathbf{u}$ will then be irrotational, $\nabla \times \mathbf{u} = 0$, and fulfill

$$\mathbf{u} = -\nabla\phi, \quad \nabla(\nabla \cdot \mathbf{u}) = \nabla^2\mathbf{u}, \quad (\mathbf{u} \cdot \nabla)\mathbf{u} = \nabla\left(\frac{\mathbf{u}^2}{2}\right), \tag{2.1}$$

where $\phi$ is a scalar velocity potential. The conservation of momentum for a fluid element can be written as

$$\frac{\partial}{\partial t}(-\nabla\phi) + (\mathbf{u} \cdot \nabla)\mathbf{u} = -\frac{\nabla p}{\rho} + \eta\frac{\nabla^2\mathbf{u}}{\rho} + \left(\frac{\zeta + \frac{1}{3}\eta}{\rho}\right)\nabla(\nabla \cdot \mathbf{u}), \tag{2.2}$$

([11, equation 2a]) where $p$ is the pressure, $\rho$ is the density of the liquid and $\eta$ and $\zeta$ are viscosity constants. The two viscosity constants can, when considered constant, be written in terms of the bulk-viscosity $\mu$ as $\mu = \frac{3}{4}\zeta + \eta$. Together with equation (2.1), equation (2.2) can be written as

$$\frac{\partial}{\partial t}(-\nabla\phi) + \nabla\left(\frac{\mathbf{u}^2}{2}\right) = -\frac{\nabla p}{\rho} + \frac{4\mu\nabla(\nabla\cdot\mathbf{u})}{3\rho}. \tag{2.3}$$

The last term in equation (2.3) can be disregarded and integration gives the Bernoulli equation:

$$-\frac{\partial\phi}{\partial t} + \frac{\mathbf{u}^2}{2} = -\int_{p_\infty}^{p}\frac{\mathrm{d}p}{\rho}, \tag{2.4}$$

given that the velocity $\mathbf{u}$ and the velocity potential $\phi$ vanishes infinitely far away, the pressure at an infinite distance $p_\infty$ is constant and the density $\rho$ can be expressed solely in terms of the pressure $p$.

By use of the entalpi $h$ the right hand side of equation (2.4) can be rewritten to

$$h = h(p) = \int_{p_\infty}^{p}\frac{\mathrm{d}p}{\rho} \;\Rightarrow\; -\frac{\partial\phi}{\partial t} + \frac{\mathbf{u}^2}{2} = -h. \tag{2.5}$$

We shall now trust Kirkwood and Bethe and use their most essential observation: the quantity $G(r) = r(h + (\mathbf{u}/2))$, called the kinetic entalpi, will propagate outwards with the velocity $(c + \mathbf{u})$ where $c$ is the local sound velocity and $\mathbf{u}$ is the particle velocity. The observation can be written as

$$\frac{\partial}{\partial t}\left[r\left(h + \frac{\mathbf{u}^2}{2}\right)\right] + (c+\mathbf{u})\frac{\partial}{\partial r}\left[r\left(h + \frac{\mathbf{u}^2}{2}\right)\right] = 0. \tag{2.6}$$

Using the particle differential $D/Dt = \partial/\partial t + \mathbf{u}\partial/\partial r$ equation (2.6) can be written as

$$\frac{D}{Dt}\left[r\left(h + \frac{\mathbf{u}^2}{2}\right)\right] + c\frac{\partial}{\partial r}\left[r\left(h + \frac{\mathbf{u}^2}{2}\right)\right] = 0$$

or with further calculation as

$$r\frac{Dh}{Dt} + c\mathbf{u}\frac{D\mathbf{u}}{Dt} + (c+\mathbf{u})\left(h + \frac{\mathbf{u}^2}{2}\right) + rc\frac{\partial h}{\partial r} + rc\mathbf{u}\frac{\partial\mathbf{u}}{\partial r} = 0. \tag{2.7}$$

The conservation of mass together with $c^2 = \mathrm{d}p/\mathrm{d}\rho$, $\mathrm{d}p/\rho = \mathrm{d}h$ and the spherical symmetry gives

$$\begin{aligned}\nabla\cdot\mathbf{u} = -\frac{1}{\rho}\frac{D\rho}{Dt} \overset{\mathbf{u}=\mathbf{u}(r)}{\Rightarrow} \frac{1}{r^2}\frac{\partial}{\partial r}\left(\frac{\mathbf{u}}{r^2}\right) = -\frac{1}{\rho}\frac{D\rho}{Dt} \overset{\rho=\rho(p)}{\Rightarrow}\\ \frac{\partial\mathbf{u}}{\partial r} + \frac{2\mathbf{u}}{r} = -\frac{\mathrm{d}\rho}{\mathrm{d}p}\frac{\mathrm{d}h}{\mathrm{d}p}\frac{Dp}{Dt} \overset{h=h(p)}{\Rightarrow} \frac{\partial\mathbf{u}}{\partial r} + \frac{2\mathbf{u}}{r} = -\frac{1}{c^2}\frac{Dh}{Dt}.\end{aligned} \tag{2.8}$$

With use of the particle derivative the conservation of momentum (2.2) can be written as

$$\frac{\partial}{\partial t}\frac{\partial}{\partial r}(-\phi)+\frac{\partial}{\partial r}\frac{\mathbf{u}^2}{2}=-\frac{\partial h}{\partial r}\;\Rightarrow\;\frac{\partial \mathbf{u}}{\partial t}+\mathbf{u}\frac{\partial \mathbf{u}}{\partial r}=-\frac{\partial h}{\partial r}\;\Rightarrow\;\frac{\partial h}{\partial r}=-\frac{D\mathbf{u}}{Dt}. \quad (2.9)$$

By use of the expressions for $\partial\mathbf{u}/\partial r$ from (2.8) and for $\partial h/\partial r$ from (2.7) in equation (2.9), the total equation describing the movement of a liquid element is

$$r\frac{Dh}{Dt}\left(1-\frac{\mathbf{u}}{c}\right)+ch\left(1+\frac{\mathbf{u}}{c}\right)-rc\frac{D\mathbf{u}}{Dt}\left(1-\frac{\mathbf{u}}{c}\right)-\frac{3}{2}c\mathbf{u}^2\left(1-\frac{\mathbf{u}}{3c}\right)=0. \quad (2.10)$$

Next we derive the thermodynamic equations for the liquid. The empirical Tait-equation for isentropic compression of a fluid is

$$\left(\frac{p+B}{p_\infty+B}\right)=\left(\frac{\rho}{\rho_\infty}\right)^\gamma, \quad (2.11)$$

where $B$ and $\gamma$ are constants which are given by the particular fluid ($B=3000$ atm and $\gamma=7$ for water), $p_\infty$ is the unperturbed hydrostatic pressure and $\rho_\infty$ the unperturbed density in the liquid. Equation (2.11) gives the following expression for the sound velocity in the liquid:

$$c^2=\frac{\mathrm{d}p}{\mathrm{d}\rho}=\frac{\mathrm{d}}{\mathrm{d}\rho}[(p_\infty+B)\left(\frac{\rho}{\rho_\infty}\right)^\gamma-B]=\frac{\gamma(p+B)}{\rho}=\frac{\gamma(p+B)}{\rho_\infty}\left(\frac{p+B}{p_\infty+B}\right)^{-1/\gamma}. \quad (2.12)$$

Hence the unperturbed sound velocity is given by

$$c_\infty^2=\frac{\gamma(p_\infty+B)}{\rho_\infty},$$

which together with equation (2.12) gives

$$c=c_\infty\left(\frac{p+B}{p_\infty+B}\right)^{\frac{\gamma-1}{2\gamma}}.$$

Equation (2.11) makes equation (2.5) integrable:

$$h=\int_{p_\infty}^{p}\left(\frac{p+B}{p_\infty+B}\right)^{-(1/\gamma)}\frac{\mathrm{d}p}{\rho_\infty}=\frac{\gamma(p_\infty+B)}{(\gamma-1)\rho_\infty}\left[\left(\frac{p+B}{p_\infty+B}\right)^{(\gamma-1)/\gamma}-1\right]. \quad (2.13)$$

At the bubble wall we write the variables $r$, $\mathbf{u}$, $c$ and $h$ with capital letters and the particle derivative becomes the time derivative since we follow the

movement of the liquid. The application of equation (2.10) at the bubble wall gives

$$R\dot{\mathbf{U}}\left(1-\frac{\mathbf{U}}{C}\right)+\frac{3}{2}\mathbf{U}^2\left(1-\frac{\mathbf{U}}{3C}\right)=H\left(1+\frac{\mathbf{U}}{C}\right)+\frac{R\dot{H}}{C}\left(1-\frac{\mathbf{U}}{C}\right). \quad (2.14)$$

The thermodynamic equations for the gas in the cavity is mainly derived from the ideal gas law. Still the heat transfer process is considered to be too slow for the relatively fast bubble oscillation, but we must now take into account that the amount of gas in the bubble is non-constant. The delayed release of the gas is assumed to take place with a constant velocity $\dot{n}$ over a period of time $\tau$:

$$\dot{n}=\frac{n_{tot}-n_i}{\tau},$$

where $n_{tot}$ is the total amount of gas and $n_i$ is the amount of gas initialized in the cavity. The ideal gas-law gives, when the variable amount of gas in the cavity is accounted for, the following expression for $\dot{T}$. From $\dot{E}_u = c_V(\dot{n}T + n\dot{T}) = -P\dot{V}$ we get

$$\dot{T}=\frac{R_gT\dot{n}-P\dot{V}}{c_Vn}.$$

As for the variables in equation (2.14) the pressure, the temperature and the volume of the bubble is written with capital letters. The ideal gas law leads to

$$P=\frac{nR_gT}{V},\quad \dot{P}=\left[\frac{\dot{n}}{n}+\frac{\dot{T}}{T}-\frac{\dot{V}}{V}\right]P.$$

The derivative of the entalpi $\dot{H}$ is obtained from derivation of equation (2.13):

$$\dot{H}=\frac{\dot{P}}{\rho}=\left(\frac{P+B}{p_\infty+B}\right)^{-\frac{1}{\gamma}}\frac{\dot{P}}{\rho_\infty},$$

and completes the set of equations. The initial conditions are

$$R(0)=\left(\frac{3V_0}{4\pi}\right)^{\frac{1}{3}},\quad T(0)=T_0,\quad P(0)=\frac{n_i}{n_{tot}}P_0,\quad U(0)=U_0,$$

since $P_0$ is the pressure when all of all the gas is in the bubble, not just the initial simulated amount. The velocity is given a value $U_0 \neq 0$ because we can not allow gas to be inserted without expanding the bubble. That would lead to unrealisticly high temperatures and pressure in the bubble.

The simulation actually starts a little later than the exact time of the airgun blast thus this is a credible consequence.

The far-field presser is calculated from the propagation of the kinetic entalpy and is given by

$$p(r,t) - p_\infty = \frac{R}{r\rho_\infty}\left(H + \frac{\dot{R}^2}{2}\right), \tag{2.15}$$

where $r$ is the distance to the center of the bubble.

### 2.1.2 Dimensionless form

To improve the conditioning of the system, a rewriting of the KB-equation to dimensionless variables is done with the following changes:

$$R \rightarrow R_m y_1, \quad t \rightarrow R_m \left(\frac{\rho_\infty}{P_a}\right)^{\frac{1}{2}} \hat{t} = \tilde{t}\hat{t}, \quad T \rightarrow T_0 y_2, \quad n \rightarrow n_{tot} y_4, \tag{2.16}$$

where $R_m$ is the maximum bubble radius, $\rho_\infty$ is the hydrostatic pressure at the depth of the bubble, $P_a$ is the atmospherical pressure and $T_0$ is the initial temperature in the bubble. This scaling decides the scaling of the remaining variables:

$$U \rightarrow \frac{R_m}{\tilde{t}} y_3, \quad \rho \rightarrow \rho_\infty \hat{\rho}, \quad P \rightarrow P_a \hat{P}, \quad H \rightarrow \left(\frac{R_m}{\tilde{t}}\right)^2 \hat{H}, \quad C \rightarrow \frac{R_m}{\tilde{t}} \hat{C}$$

and the scaling of the constants $p_\infty \rightarrow P_a \hat{p_\infty}$, $c_\infty \rightarrow \frac{R_m}{\tilde{t}} \hat{c_\infty}$ which is not strictly necessary, but makes it easier to keep control of the dimensions. The

total set of equations becomes:

$$\hat{P} = \frac{3R_gT_0}{4\pi P_a R_m^3}\frac{y_4 y_2}{y_1^3}\,, \tag{2.17a}$$

$$\dot{\hat{P}} = \left[\frac{\dot{y_4}}{y_4} + \frac{\dot{y_2}}{y_2} - \frac{3y_3}{y_1}\right]\hat{P}\,, \tag{2.17b}$$

$$\dot{\hat{H}} = \left(\frac{\hat{P}+\hat{B}}{\hat{p_\infty}+\hat{B}}\right)^{-\frac{1}{\gamma}}\frac{\dot{\hat{P}}}{\hat{\rho_\infty}}\,, \tag{2.17c}$$

$$\hat{H} = \frac{\gamma(\hat{p_\infty}+\hat{B})}{(\gamma-1)}\left[\left(\frac{\hat{P}+\hat{B}}{\hat{p_\infty}+\hat{B}}\right)^{\frac{\gamma-1}{\gamma}} - 1\right]\,, \tag{2.17d}$$

$$\hat{C} = \hat{c_\infty}\left(\frac{\hat{P}+\hat{B}}{\hat{p_\infty}+\hat{B}}\right)^{\frac{\gamma-1}{2\gamma}}\,, \tag{2.17e}$$

$$\dot{y_1} = y_3\,, \tag{2.17f}$$

$$\dot{y_2} = \frac{R_g}{c_V}\frac{\dot{y_4}y_2}{y_4} - \frac{3R_g}{C_v}\frac{y_2 y_3}{y_1}\,, \tag{2.17g}$$

$$\dot{y_3} = \frac{\hat{H}\left(1+\frac{y_3}{\hat{C}}\right) + \frac{y_1\dot{\hat{H}}}{\hat{C}}\left(1-\frac{y_3}{\hat{C}}\right) - \frac{3}{2}y_3^2\left(1-\frac{y_3}{3\hat{C}}\right)}{y_1\left(1-\frac{y_3}{\hat{C}}\right)}, \tag{2.17h}$$

$$\dot{y_4} = \begin{cases}\frac{1-y_4^i}{\hat{\tau}}, & \text{if } \hat{t} \le \hat{\tau}\\ 0, & \text{otherwise}\end{cases} \tag{2.17i}$$

where $y_4^i$ is the dimensionless fraction $\frac{n_i}{n_{tot}}$. The initial conditions needed for solving (2.17) is

$$y_1(0) = \frac{1}{R_m}\left(\frac{3V_0}{4\pi}\right)^{\frac{1}{3}},\ y_2(0) = 1,\ \hat{P(0)} = \frac{P_0 y_4^i}{P_a},\ y_3(0) = \frac{R_m U_0}{\tilde{t}},\ y_4(0) = y_4^i.$$

The equations are in fact implicit since $\dot{\hat{P}}$ depends on $\dot{y_2}$ and $\dot{y_4}$, and $\dot{y_2}$ depends on $\dot{y_4}$ so $y' = f(t, y, y')$, but since $\dot{y_2}$ does not depend on $\dot{\hat{P}}$ and $\dot{y_4}$ is constant for $\hat{t} \neq \hat{\tau}$ this fact can be avoided simply by calculating the variables in a certain order, and an explicit ordinary differential equation $y' = f(t, y)$ is to be solved.

### 2.1.3 Discussion of assumptions

The Kirkwood-Bethe equation (KB-equation) is derived with some physical assumptions on the way. The assumption of spherical symmetry is not

very accurate. High speed photography of the air bubble [8] clearly shows a fractal surface and a somewhat elliptic shape. Both gravity and general chaos in addition to the fact that the airgun itself is in the way contribute to the irregular shape of the bubble. On the other hand the far-field pressure measured from an airgun blast is close to spherical (without any additional reflections e.g. from the sea surface), and it is this pressure signature we are interested in. Thus it can be simulated by a spherical approach, and the simplification is acceptable. The alternative would anyhow demand very complicated physics and mathematics, and deriving the equations would be very difficult.

The last term in equation (2.3) is disregarded assuming the viscosity and the compressibility to be small. Inserting the magnitude of the variables and constants involved,

$$u \approx 10,\ r \approx 10^{-1},\ \mu \approx 10^{-3},\ \rho \approx 10^{3},\ p \approx 10^{5},\ t \approx 10^{-1},$$

into the equation results in the following term magnitudes

$$10^2 + 10^3 = 10^3 + 10^{-3},$$

which clearly justifies the neglection of the last term.

The heat transfer process has been considered to be too slow to be taken into account. The heat equation can be written as

$$\frac{\partial T}{\partial t} = \frac{k}{\rho c}\nabla^2 T,$$

where $k$ is the conductivity, $\rho$ the density, $c$ is the specific heat capacity and $T$ is the temperature. The constant $\kappa = \frac{k}{\rho c}$ decides the ratio of absorption and transmission of heat in the material and has the dimension $[L]^2[T]^{-1}$. The distance $L$ which a significant part of an outer temperature change has traveled after a time $t$ will then be proportional to $\sqrt{\kappa t}$ [6]. The oscillation of the bubble has a period of approximately $10^{-2}$ s. Hence the change of temperature in the bubble spreads $L \approx \sqrt{10^{-7} \cdot 10^{-2}} < 10^{-4}$ within this time period. Since both the heat expansion coefficient for water and the total amount of transfered energy is so small, the heat transfer process can safely be neglected.

### 2.1.4 Empirical adjustments

Measurements of airgun pressure signatures have proven the KB equation inaccurate. There are several physical phenomena that dampen the oscillation process. In real life the system looses energy and dies out more quickly

than what the solution of the equations yields. Several attempts at finding the most significant energy loss mechanism have ended up mainly depending on empirical constants. One example is the process of state transfer of mass between gas and liquid. When the bubble expands, the temperature drops and the humidity in the gas condenses on the bubble wall. When the bubble contracts, the temperature rises and water evaporate from the bubble wall. This process requires energy and contributes to the damping of the oscillation. Although we calculate with a fractal structure of the surface of the bubble, it does not fill the gap between the theoretical and measured results. It is therefore common to add purely empirical terms to the KB equation instead of a physical approach. The equation (2.14) is replaced with

$$R\dot{\mathbf{U}}\left(1-\frac{\mathbf{U}}{C}\right)+\frac{3}{2}\mathbf{U}^2\left(1-\frac{\mathbf{U}}{3C}\right)=H\left(1+\frac{\mathbf{U}}{C}\right)+\frac{R\dot{H}}{C}\left(1-\frac{\mathbf{U}}{C}\right)-\alpha\mathbf{U}+\beta\mathbf{U}^2,$$

where $\alpha$ and $\beta$ are constants adjusted for each airgun. The pressure wave signature calculated with this equation is very close to measured signatures.

## 2.2 Coupled airguns

As presented in the introduction, the airguns are coupled in clusters where they interact with each other, and several of these clusters are lined up so their transmitted signals interfere to create a desirable joint pressure output waveform in the far-field. The interaction between the two clustered airguns is modeled by adding the pressure from the neighboring airgun to the hydrostatic pressure. This is a valid physical approach as long as the airguns are at least some distance apart and at a certain depth. The critical values for the distance and the depth are decided empirically and assumed to be "small enough" in our simulations even though it might not be true.

Let the solution of two coupled airguns be $u(t)$ and $v(t)$ respectively. The equations that need to be solved can then be written as:

$$\begin{aligned} u'(t) &= g(t, u(t), v(t-\tau_1), u(t-\tau_2), v(t-\tau_3)) \\ v'(t) &= h(t, v(t), u(t-\tau_1), v(t-\tau_2), u(t-\tau_3)) \\ \Rightarrow \quad y'(t) &= f(t, y(t), y(t-\tau_1), y(t-\tau_2), y(t-\tau_3)), \end{aligned} \tag{2.18}$$

where $\tau_1$ is the time it takes the propagating pressure wave to travel between the airguns, $\tau_2$ is the time it takes the pressure wave to travel from the airgun to the surface and back to the same airgun and $\tau_3$ is the time the pressure wave takes to travel from one airgun, to the surface and to the other airgun. The velocity of the propagating waves is assumed to be constant, and the delays are calculated from the distance between the airguns and the distance

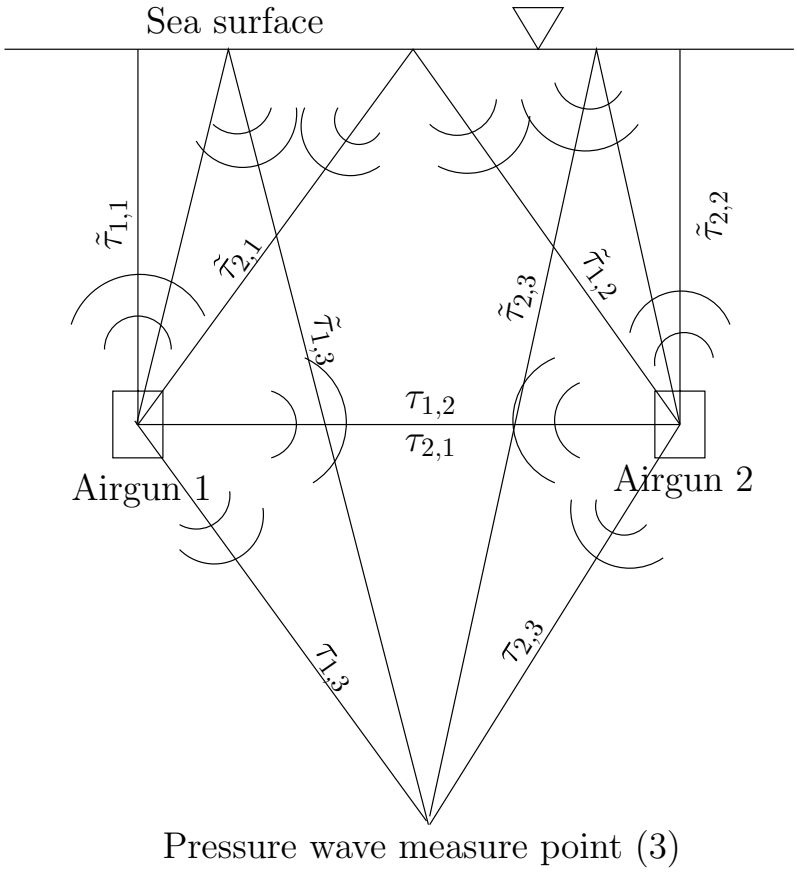


Figure 2.1: The distances between the two airguns in the cluster which must be taken into account when simulating the joint output pressure pulse. The $\tau_{i,j}$ is the time the pressure wave takes to propagate from $i$ to $j$ and $\tilde{\tau}$ denotes the time over distances which includes reflection from the sea surface.

between the airguns and the surface. The delays involved are illustrated in figure 2.1 where $\tau_1 = \tau_{1,2} = \tau_{2,1}$, $\tau_2 = \tilde{\tau}_{1,1} = \tilde{\tau}_{2,2}$ and $\tau_3 = \tilde{\tau}_{1,2} = \tilde{\tau}_{2,1}$ and the remaining delays $\tilde{\tau}_{1,3} = \tilde{\tau}_{2,3}$ and $\tau_{1,3} = \tau_{2,3}$ are used to calculate the joint output pressure wave.

The delayed pressure will be included in (2.17) by replacing $\hat{p_\infty}$ with

$$\hat{p_{dyn}} = \hat{p_\infty} + \hat{p_{del}},$$

where $\hat{p_{del}}$ is the joint pressure wave hitting the airgun in question consisting of the neighboring airgun's pressure, the ghost-pressure and the neighboring airgun's ghost-pressure.

The reflection at the sea surface inverses the wave. The amplitude is preserved according to a reflection coefficient of $\gamma \in [-1.0, -0.8]$ [3]. Although

a reflection coefficient of $\gamma = -1.0$ seldom is obtained, it is often used for simplicity.

# 3 Numerical methods for solving interacting bodies with delays

The equations describing the system of interacting airguns (2.18) are delay differential equations (DDEs). The theory behind these equations will only be discussed briefly here and the reader is referred to Bellen and Zennaro [2] for a thorough introduction. Different numeric solvers will be presented, some of these described in [2] and the remaining introduced by Tavernini and Cryer [4] and rewritten and exemplified by Maset, Torelli and Vermiglio [9].

## 3.1 Delay differential equations

A general ordinary differential equation (ODE) can be extended to include dependence on the solution at a retarded time. The most general form is the retarded functional differential equation (RFDE)

$$y'(t) = f(t, y_t), \tag{3.1}$$

where $y_t = y_t(\theta) = y(t+\theta)$, $\theta \in [-r, 0]$, is a function belonging to the Banach space $C = \mathcal{C}^0([-r, 0], \mathbb{R}^d)$ of continuous functions $[-r, 0] \to \mathbb{R}^d$, $r \in [0, \infty)$ and the function $f : \Omega \to \mathbb{R}^d$ where $\Omega \subset \mathbb{R} \times C$.

As an initial value problem (IVP) where the derivative $y'(t)$ is to be thought of as the right hand side derivative $y'(t)^+$, the IVP (3.1) can be written as

$$\begin{cases} y'(t) = f(t, y_t),\ t_0 \le t, \\ y_{t_0} = y(t_0 + \theta) = \Phi(\theta), \end{cases} \tag{3.2}$$

where $\Phi \in C$ is the initial function.

If the splitting

$$f(t, \phi) = f(t, \phi(0), \phi|_{[-r,-r_1]}),\ r_1 \in (0, r] \tag{3.3}$$

is possible, equation (3.2) can be written as

$$\begin{cases} y'(t) = f(t, y(t), w_t),\ t_0 \le t, \\ y(t) = g(t),\ t \le t_0, \end{cases} \tag{3.4}$$

where $w_t \in C$ is given by

$$w_t = w_t(\theta) = \begin{cases} y(t+\theta), & t_0 \le t + \theta \\ g(t+\theta), & t + \theta \le t_0, \end{cases} \tag{3.5}$$

for $\theta \in [-r, -r_1]$ so the IVP (3.4) can locally be viewed as an ODE.

If $f$ only depends on the solution $y(t)$ at a finite number of points in time $t - \tau_i$ where $\tau_i$ are the delays, and the equation does not need to depend on the present time, then the IVP (3.4) can be written as

$$\begin{cases} y'(t) = f(t, y(t-\tau_1), \ldots, y(t-\tau_n)), \ t_0 \leq t, \\ y(t) = g(t), \ t \leq t_0, \end{cases} \tag{3.6}$$

where $\tau_i \in \mathbb{R}^+$, $f : [t_0, t_f] \times \mathbb{R}^d \times \cdots \times \mathbb{R}^d \to \mathbb{R}^d$, $[t_0, t_f] \subset \mathbb{R}$ is the integration interval, and $g : [t_0 - \max_{1 \leq i \leq n} \tau_i, t_0] \to \mathbb{R}^d$. The delays $\tau_i$ can also be functions of both time and state, but only constant delays occur in the airgun equations so these will have our main focus. The two latter IVPs (3.4) and (3.6) will be referred to as DDEs.

The exact solution of a DDE can be obtained by splitting the original equation into ODEs. Hence the theory for existence and uniqueness of the solution of a DDE can be obtained directly from ODE theory (see [5]) and the following conditions need to be fulfilled to ensure existence and uniqueness of the solution of (3.4):

1. $f(t, u, v)$ continuous with respect to $t$,
2. $f(t, u, v)$ Lipschitz continuous with respect to $u$ and $v$ in $[t_0, t_0 + h] \times U \times C$ for some $h > 0$ where $U \subseteq \mathbb{R}^d$ is a neighborhood of $g(t_0)$ ,
3. $g(t)$ Lipschitz continuous with respect to $t$.

For equation (3.6) the second condition above is replaced by

2. $f(t, u)$ Lipschitz continuous with respect to $u$ in $[t_0, t_0 + h] \times U$ for some $h > 0$ where $U \subseteq \mathbb{R}^d \times \cdots \times \mathbb{R}^d$ is a neighborhood of $(g(t_0 - \tau_1), \ldots, g(t_0 - \tau_n))$.

### 3.1.1 Breaking points

The discontinuities in the derivatives of the input arguments of the DDE will limit the smoothness of the solution. For a DDE of the type (3.6) with $\tau_1 = 0$, $\tau_2 = \tau$ and $f, g \in \mathcal{C}^\infty$, the assumption $g'(t_0)^- \neq y'(t_0)^+ = f(t_0, g(t_0), g(t_0 - \tau))$ leads to $y(t_0) \in \mathcal{C}^0$ which affects the solution $y(t_0 + \tau)$ where

$$y''(t_0 + \tau) = f(t_0 + \tau, y(t_0 + \tau), y(t_0))(1 + y'(t_0 + \tau) + y'(t_0)).$$

Hence $y''(t_0 + \tau)^- \neq y''(t_0 + \tau)^+$ and $y(t_0 + \tau) \in \mathcal{C}^1$. The initial discontinuity restrains the smoothness of the solution at every point $\xi_j = j\tau$, called breaking points, resulting in $y(t_0 + \xi_j) \in \mathcal{C}^j$ for $j \in \mathbb{N}_0$.

In a system of equations which contains several delay arguments, the solutions smoothness may be affected by more than one delay argument at the same time. For the IVP (3.6) consider the functions

$$\alpha_i(t) = t - j\tau_i,\ j \in \mathbb{N}_0,\ i = 1, \ldots, n. \tag{3.7}$$

The breaking points $\xi_{j,i}$ will then be the points in time that fulfills $\alpha_i(\xi_{j,i}) = t_0$, such that $y(\xi_{j,i}) \in \mathcal{C}^m$ where $m$ is the smallest $j$ for all equal $\xi_{j,i}$.

For the IVP (3.4) the delays will in any case of nature of the delay dependency be calculated as from distinct values

## 3.2 Runge-Kutta methods

A DDE of the type (3.4) can be solved with a standard Runge-Kutta (RK) method with additional interpolation. We will use the ability to consider DDEs as ODEs locally (the standard approach) to construct numerical methods or to apply numerical schemes for ODEs to solve DDEs. The K-notation of an explicit RK-method (ERK) takes the from

$$K_r = f(t_m + c_r h, y_m + h_{m+1} \sum_{j=1}^{r-1} a_{r,j} K_j, w_{t_m}),\ r = 1, \ldots, s, \tag{3.8a}$$

$$y_{m+1} = y_m + h \sum_{r=1}^{s} b_r K_r, \tag{3.8b}$$

providing an approximation to the solution $y(t_{m+1})$ on the mesh $\Delta = [t_0 \ldots, t_m, t_{m+1}, \ldots, t_f]$ where $h_{m+1} = t_{m+1} - t_m > 0$ and the coefficients $A = [a_{jr}]_{j,r=1}^{s}$, the weights $b = [b_1, \ldots, b_s]$ and the abscissae $c = [c_1, \ldots, c_s]^T$ are given by the particular method.

The RK-method normally requires the exact solution to be at least $\mathcal{C}^{p+1}$, where $p$ is the order of the method, on every interval $[t_m, t_{m+1}]$, $t_m, t_{m+1} \in \Delta$. Therefore the breaking points $\xi_{l,i}$ for $l = 1, \ldots, p+1$ must be included in the mesh $\Delta$. We are only concerned with constant delays, hence the breaking points are easily located and included in the mesh a priori.

### 3.2.1 Interpolation

When $t_0 < t+\theta$ in equation (3.4) we need to approximate the solution $y(t+\theta)$ to estimate $w_{t_m}$. The discrete values obtained by the ERK method are seldom the exact points needed ($t_m \neq t + \theta$, $t_m \in \Delta$), so a dense representation $\eta(t)$ of the solution must be computed. It can be shown that if the RK method is

of order $p$ and the interpolation is of order $q$, then the discrete order obtained is $q' = \min\{p, q+1\}$, that is

$$\max_{t_i \in \Delta} ||y(t_i) - y_i|| = \mathcal{O}(h^{q'}),$$

where $y(t_i)$ is the exact solution of the DDE and $y_i$ is the numerical solution at the nodal points. The continuous order $q$ gives

$$\max_{t_0 \leq t \leq t_f} ||y(t) - \eta(t)|| = \mathcal{O}(h^q).$$

**Cubic Hermite interpolation** Cubic Hermite interpolation is an interpolation technique which is defined by finding for each interval $[t_m, t_{m+1}]$ a polynome $H(t) \in \Pi_3$ that satisfies

$$\begin{aligned} H(t_m) = f(t_m) \quad &, H'(t_m) = f'(t_m), \\ H(t_{m+1}) = f(t_{m+1}), \quad &H'(t_{m+1}) = f'(t_{m+1}). \end{aligned}$$

The polynomial will be of order $q = 3$ on each interval assuming $f \in \mathcal{C}^p$, $p \geq 4$. This interpolation technique is well suited because it only requires data from the two endpoints of the interval and the data needed is already calculated.

### 3.2.2 Overlapping

In equation (3.8a) we are evaluating $f$ at $t = t_m + c_i h$ and the interval $w_{t_m}$ is covering $[t_0 - r, t_m]$ may not contain the value $t_m + c_i h - \tau$ where $\tau \in [r_1, r]$ and where $c_i h - \tau$ is the value of $\theta$ in (3.5) of current interest. Thus if $r_1$ is small, $w_{t_m}(\theta)$ must be calculated for $\theta \in \mathbb{R}^+$. Extrapolation may be used, but to ensure high order accuracy this is a demanding task with great computational costs.

## 3.3 Continuous Runge-Kutta methods

We can use the RK-method itself to achieve the continuous extension of the discrete solution. Continuous RK-methods (CRKs) may be used and an explicit CRK (CERK) for solving equation (3.4) can be written as

$$K_r = f(t_m + c_r h_{m+1}, y_m + h_{m+1} \sum_{j=1}^{r-1} a_{r,i} K_i, w_{t_m}), \ r = 1, \ldots, s, \quad (3.9a)$$

$$y_{m+1}(\varphi) = y_m + h_{m+1} \sum_{r=1}^{s} b_r(\varphi) K_r, \ \varphi \in [0, 1], \quad (3.9b)$$

where the polynomial functions $b_r(\varphi)$ differ from the weights of the RK-methods. Only interpolation techniques of the first class will be considered (interpolation without any additional stages). The $b_r(\varphi)$ functions need to fulfill $b_r(0) = 0$, $b_r(1) = b_r$ where $b_r$ are the weights of the underlying RK-method, as well as the order criteria, derived from the standard RK theory, to ensure a certain order $q$ for any $\varphi \in [0, 1]$ (see [2, chapter 5] or [5, chapter II.6]). It can be proven that for a RK-method of order $p$ there exists a continuous extension of at least order $q = \lfloor \frac{p+1}{2} \rfloor$, but often a higher order can be achieved.

### 3.3.1 Overlapping

As for the standard RK-methods, overlapping may cause problems. The function $w_{t_m}$ can be evaluated outside the interval where a solution has been obtained by inserting

$$w_{t_m}(\alpha) = y_m + h_{m+1} \sum_{r=1}^{s} b_r(\alpha) K_r, \ \alpha = c_i h_{m+1} - \frac{\tau}{h_{m+1}}$$

where $\tau \in [r_1, r]$ is the delay of current interest. This will make explicit methods implicit which, as for extrapolation, may contribute to relatively large computational costs.

## 3.4 Collocation methods and superconvergence

A one step collocation method is an implicit CRK-method which is given by calculating the polynomial $\eta(t)$ as follows. Given $s$ distinct abscissae $c_1, \ldots, c_s \in [0, 1]$, compute $\eta(t)$ of degree $\leq s$ at every mesh interval $[t_m, t_{m+1}]$ so it satisfies

$$\eta'(t^i_{m+1}) = f(t^i_{m+1}, \eta(t^i_{m+1})), \ i = 1, \ldots, s, \ \eta(t_m) = y_m. \tag{3.10}$$

For any choice of the abscissae the order will be $p \geq s$ and the uniform order of the polynomial created will be $q = s$. If the abscissae are the shifted roots of the Legendre orthogonal polynomial, the order will be $p = 2s$. If a methods maximum reachable uniform order by means of interpolation of the first class is $\leq p - 1$ the method is called superconvergent. According to this the collocation method with the Legendre abscissae is superconvergent.

### 3.4.1 Natural continuous extension

A continuous extension obtained by an CRK-method is called a natural continuous extension (NCE) if it satisfies the orthogonal condition:

$$\| \int_{t_n}^{t_{n+1}} G(t)[z'_{n+1} - \eta'(t)] \, \mathrm{d}t \| = \mathcal{O}(h_{n+1}^{p+1})$$

for every sufficiently smooth matrix-valued function G, uniformly with respect to $n = 1, \ldots, N$. Here $z_{n+1}$ is the local solution of the local problem

$$\begin{cases} z'_{n+1}(t) = f(t, z_{n+1}(t)), \ t_n \leq t \leq t_{n+1}, \\ z_{n+1}(t_n) = y_n. \end{cases}$$

The continuous solution provided by (3.10) is a NCE.

A RK-method of order $p$ with a NCE of order $q$ will when applied to equation (3.4) with a constrained mesh $\Delta$ provide a solution of discrete order $p$ and uniform order $q' = \min\{p, q+1\}$.

A constrained mesh is a mesh where an arbitrary set of mesh points $\xi_0 = t_0 < t_1 < \cdots < t_m = \xi_1$ gives the set points in any following interval $[\xi_k, \xi_{k+1}]$ by

$$t_{km+i} = t_{(k-1)m+i} + \tau, \ i = 1, \ldots, m.$$

Hence the superconvergence of a collocation method is preserved when applied to a DDE, but only on a grid determined by the delay. A variable step size method will loose these good convergence qualities, and the same will happen when overlapping occurs [2].

## 3.5 RK methods for RFDEs

Both RK-methods with interpolation/extrapolation and CRK-methods are based on viewing the DDE as an ODE with additional delay handling. The possibility for overlapping will in those cases result in either extrapolation or an implicit method. There exist however methods that are constructed directly for RFDEs which include explicit methods that stay explicit in the case of overlapping. Of these methods we will consider the RK-methods where not only the weights $b$ from ordinary RK methods are replaced by polynomial functions as for CRK methods, but also the coefficient matrix $A$ is replaced by polynomial functions.

Consider the equation (3.2) and assume that $f$ is continuous and $f' = \frac{\mathrm{d}f}{\mathrm{d}y_t} : \Omega \to \mathcal{L}(C, \mathbb{R}^d)$ is continuous and bounded with respect to the second argument. Then for each $(\sigma, \rho) \in \Omega$ there exists a unique solution $y =$

$y(\sigma,\rho) : [\sigma - r, \bar{t}) \to \mathbb{R}^d$ of (3.2) through $(\sigma,\rho)$, where $\bar{t} = \bar{t}(\sigma,\rho) \in (\sigma,\infty]$, i.e. $y$ satisfies (3.2) for $t \in [\sigma,\bar{t})$ and $y_\sigma = \rho$ (see [9]).

A single step of size $h$ with a numeric solver is then defined for the solution $y$ through $(\sigma,\rho)$ on $[0,h]$ as an approximation of the shift $y(\sigma+\cdot)$ resulting in a continuous function $\eta(\varphi h)$:

$$\begin{aligned} \eta(\varphi h) &= \rho(0) + h\sum_{i=1}^{j-1} b_i(\varphi)K_i, \\ K_i &= f(\sigma + c_i h, Y^i_{c_i h}),\ i = 1,\dots,s \end{aligned} \tag{3.11}$$

where the *stage functions* $Y^i : [\theta, c_i h] \to \mathbb{R}^d$ are given by

$$\begin{aligned} Y^i(\alpha h) &= \rho(0) + h\sum_{j=1}^{i-1} a_{ij}(\alpha)K_j,\ \alpha \in [0,c_i], \\ Y^i(\theta) &= \rho(\theta),\ \theta \in [-r,0], \end{aligned}$$

where $A(\alpha) = [a_{ij}(\alpha)]_{i,j=1}^s$ is an $\mathbb{R}^{s\times s}$-valued polynomial function such that $A(0) = 0$. The existence and uniqueness of the vector $K = (K_1^T,\dots,K_s^T)^T$ is proved in [9].

The construction of the method (3.11) is quite different from CRK-methods, yet if it is applied ta a DDE and the step size is smaller than any delay, the method behaves exactly as the CRK-method (3.9). In the case of overlapping, the solution will differ from an implicit CRK-method since $Y^i \neq \eta$, $i = 1,\dots,s$ in general.

The airgun equations are clearly possible to split as in (3.3) but the short distance between the clustered airguns may result in overlapping and the RFDE methods may prove suited to achieve efficient integration.

### 3.5.1 Global order

Two methods of different order may be used to constrain the step size $h$ such that the error is smaller than some error bound. If the advancing method has discrete order $p$ and uniform order $q = p-1$ and the error controlling method has discrete order $p' = p-1$, then the global error $E$ normally obeys $E \leq \mathcal{O}(TOL)$ for some upper tolerance bound $TOL$ if the step size at each step satisfies

$$\frac{||\tilde{y}_{m+1} - y_{m+1}||}{h_{m+1}} \leq TOL, \tag{3.12}$$

where $\tilde{y}_{m+1}$ and $y_{m+1}$ are the approximated values of the solution $y(t_{m+1})$ achieved by the advancing and the error controlling method respectively.

Controlling the sole discrete error may in some cases be insufficient to ensure the global error bound, and a uniform error test must then be applied as well.

## 3.6 Matlab methods

Matlab has several solvers for both ODEs and DDEs, and two of these, ode45 and dde23, has been used to solve the Rayleigh- and the KB-equation.

### 3.6.1 ode45

ode45 is an ERK-method of order $p = 5$ which uses a method of order $p' = 4$ to estimate the local error in every step. The two methods are a Dormand-Prince pair.

### 3.6.2 dde23

dde23 is a standard ERK method of discrete order $p = 3$ with an error controlling ERK-method of order $\tilde{q} = 2$. To obtain the continuous extension of the solution, it uses a method based on cubic Hermite interpolation (see section 3.2.1).

When overlapping occurs, an approximate value of $w_{t_m}(\theta)$ in equation (3.5) is obtained by extrapolation and used as a start value for an iteration consisting of two steps. First step is obtaining a new value of $(y_{m+1}, y'_{m+1})$ by use of the advancing ERK-method and the second step is calculating a new $w_{t_m}(\theta)$ by interpolation. The two steps are carried out five and four times respectively.

The solver is quite robust and handles both discontinuities and jumps in the solution as long as their occurrence is possible to determine a priori.

# 4 Implementation

The derived differential equations and the numerical methods have been implemented in Matlab (version 7.1.0.183 (R14) with service pack 3). The Rayleigh equation (A.7) and the Kirkwood-Bethe equation (2.17) have been solved with ode45, dde23, RK-methods with linear interpolation as described in section 3.2 as well as RFDE-methods of the type described in section 3.5.

## 4.1 RFDE methods

An efficient code should be implemented with variable step size, and the error tolerance bounds described in section 3.5.1 would assure both the uniform and discrete accuracy of the global solution. My code has been implemented with constant step size. The ability to investigate the error as a function of the step size will naturally not diminish. The code will be significantly less efficient than with variable step size, but the efficiency can still be investigated.

The implemented code consists of a main solver, a function for storing/fetching solution values in/from a separate array and the different methods given by their respective coefficients. The main solver gets the coefficients from the particular method, stores the values needed for obtaining the uniform solution at each step in the separate array and fetches the values needed for computing the delay values. The solver will be referred to as *ddeConst* and the particular method used will be specified additionally.

The stored values in the separate array are not the K-values from each step. A rewriting of the expression for the continuous solution has been done to store fewer values. For a CRK method or an RFDE method the continuous solution obtained from the stored values (no overlapping) is given by

$$y_{m+1}(\varphi) = y_m + h\sum_{i=1}^{s} b_i(\varphi)K_i,$$

where $s$ is the number of stages while the $b_i(\varphi) = b_{i1}\varphi + \cdots + b_{ik}\varphi^k$ are polynomials with $k \leq p$ where $p$ is the order of the method. By storing the coefficient for every power of $\varphi$ the same solution can be calculated from

$$y_{m+1}(\varphi) = y_m + h\sum_{j=1}^{k} B_j\varphi^j,\ B_j = \sum_{i=1}^{s} b_{ij}K_i.$$

As introduced in section 3.1.1 the breaking points must be included in the mesh. This is done by a simple overruling of the step length. Since the delays are constant it is easy to calculate for how large a multiple of the $\tau$ values this needs to be done.

RFDE methods of discrete order 1, 2, 3 and 4 have been implemented. The first order method is the Euler method which only evaluates the function at the start point of each step thus overlapping will never occur. The CRK-version and the RFDE-version of Eulers method is identical and given in the Butcher tableau in table 4.1. The second order method is the Heun method

| | |
|---|---|
| 0 | 0 |
| | $\varphi$ |

Table 4.1: RFDE method of order 1 (Euler).

given in table 4.2. The third order method is a four-stage method given in

| | | |
|---|---|---|
| 0 | 0 | 0 |
| 1 | $\alpha$ | 0 |
| | $\varphi - \frac{1}{2}\varphi^2$ | $\frac{1}{2}\varphi^2$ |

Table 4.2: RFDE method of order 2 (Heun).

table 4.3. I have implemented two different methods of order 4. One with six

| | | | | |
|---|---|---|---|---|
| 0 | 0 | 0 | 0 | 0 |
| 1 | $\alpha$ | 0 | 0 | 0 |
| $\frac{1}{2}$ | $\alpha - \frac{1}{2}\alpha^2$ | $\frac{1}{2}\alpha^2$ | 0 | 0 |
| 1 | $\alpha - \frac{1}{2}\alpha^2$ | $\frac{1}{2}\alpha^2$ | 0 | 0 |
| | $\varphi - \frac{3}{2}\varphi^2 + \frac{2}{3}\varphi^3$ | 0 | $2\varphi^2 - \frac{4}{3}\varphi^3$ | $-\frac{1}{2}\varphi^2 + \frac{2}{3}\varphi^3$ |

Table 4.3: RFDE method of order 3.

stages given in table 4.4 and one with seven stages given in table 4.5 where the $b_i(\varphi)$ functions are given by

$$
\begin{aligned}
b_1(\varphi) &= \varphi - \frac{11}{4}\varphi^2 + 3\varphi^3 - \frac{9}{8}\varphi^4, \\
b_5(\varphi) &= \frac{9}{2}\varphi^2 - \frac{15}{2}\varphi^3 + \frac{27}{8}\varphi^4, \\
b_6(\varphi) &= -\frac{9}{4}\varphi^2 + 6\varphi^3 - \frac{27}{8}\varphi^4, \\
b_7(\varphi) &= \frac{1}{2}\varphi^2 - \frac{3}{2}\varphi^3 + \frac{9}{8}\varphi^4.
\end{aligned}
$$

All these methods are developed from collocation methods presented by Tavernini in [4] and written out as explicit RK-methods for RFDEs by Maset, Torelli and Vermiglio in [9].

| | | | | | | |
|---|---|---|---|---|---|---|
| 0 | 0 | 0 | 0 | 0 | 0 | 0 |
| 1 | $\alpha$ | 0 | 0 | 0 | 0 | 0 |
| $\frac{1}{2}$ | $\alpha - \frac{1}{2}\alpha^2$ | $\frac{1}{2}\alpha^2$ | 0 | 0 | 0 | 0 |
| 1 | $\alpha - \frac{1}{2}\alpha^2$ | $\frac{1}{2}\alpha^2$ | 0 | 0 | 0 | 0 |
| $\frac{1}{2}$ | $\alpha - \frac{3}{2}\alpha^2 + \frac{2}{3}\alpha^3$ | 0 | $2\alpha^2 - \frac{4}{3}\alpha^3$ | $-\frac{1}{2}\alpha^2 + \frac{2}{3}\alpha^3$ | 0 | 0 |
| 1 | $\alpha - \frac{3}{2}\alpha^2 + \frac{2}{3}\alpha^3$ | 0 | $2\alpha^2 - \frac{4}{3}\alpha^3$ | $-\frac{1}{2}\alpha^2 + \frac{2}{3}\alpha^3$ | 0 | 0 |
| | $\varphi - \frac{3}{2}\varphi^2 + \frac{2}{3}\varphi^3$ | 0 | 0 | 0 | $2\varphi^2 - \frac{4}{3}\varphi^3$ | $-\frac{1}{2}\varphi^2 + \frac{2}{3}\varphi^3$ |

Table 4.4: RFDE method of order 4 (with six stages).

| | | | | | | | |
|---|---|---|---|---|---|---|---|
| 0 | 0 | 0 | 0 | 0 | 0 | 0 | 0 |
| 1 | $\alpha$ | 0 | 0 | 0 | 0 | 0 | 0 |
| $\frac{1}{2}$ | $\alpha - \frac{1}{2}\alpha^2$ | $\frac{1}{2}\alpha^2$ | 0 | 0 | 0 | 0 | 0 |
| 1 | $\alpha - \frac{1}{2}\alpha^2$ | $\frac{1}{2}\alpha^2$ | 0 | 0 | 0 | 0 | 0 |
| $\frac{1}{3}$ | $\alpha - \frac{3}{2}\alpha^2 + \frac{2}{3}\alpha^3$ | 0 | $2\alpha^2 - \frac{4}{3}\alpha^3$ | $-\frac{1}{2}\alpha^2 + \frac{2}{3}\alpha^3$ | 0 | 0 | 0 |
| $\frac{2}{3}$ | $\alpha - \frac{3}{2}\alpha^2 + \frac{2}{3}\alpha^3$ | 0 | $2\alpha^2 - \frac{4}{3}\alpha^3$ | $-\frac{1}{2}\alpha^2 + \frac{2}{3}\alpha^3$ | 0 | 0 | 0 |
| 1 | $\alpha - \frac{3}{2}\alpha^2 + \frac{2}{3}\alpha^3$ | 0 | $2\alpha^2 - \frac{4}{3}\alpha^3$ | $-\frac{1}{2}\alpha^2 + \frac{2}{3}\alpha^3$ | 0 | 0 | 0 |
| | $b_1(\varphi)$ | 0 | 0 | 0 | $b_5(\varphi)$ | $b_6(\varphi)$ | $b_7(\varphi)$ |

Table 4.5: RFDE method of order 4 (with seven stages).

## 4.2 Kirkwood-Bethe equation

The general implementation of the KB-equation is straight forward as long as the calculation of the equations is executed in the right order as described in section 2.1.2.

The far-field pressure given in equation (2.15) is calculated from the delayed values for every evaluation of the KB-equation, but not integrated along with the variables of which it depends. The pressure transmitted from the bubble is calculated from the solution of the KB-equation after ended integration, and filtered with a low-pass filter (0-128Hz). Variation of the filter coefficients gave dramatical changes in the pressure waves primary peak amplitude. The filter has therefore been calibrated to fit measured data collected by Langhammer in [8].

### 4.2.1 Two-gun cluster

When more than one airgun are simulated at the same time and the interacting pressure waves are included, the system of equations will be of size $4N$ where $N$ is the number of airguns. The scaling of the variables is done according to the largest gun, or the gun with the largest initial pressure which will generate the largest maximum bubble radius.

The implemented code only supports two airguns, where the time of release is equal for both the airguns. This excludes the opportunity to explore pressure signatures which mainly consist of a primary peak and where the following pressure waves interfere destructively, but normally we would need several clusters to achieve a good joint output pressure waveform, and therefore this is not a great loss. The airguns are placed at the same depth with the possibility of varying the distance between them.

The given step size is applied in the dimensionless time domain. The rescaling of the time variable as given in 2.16 has been kept constant for all simulations at the same depth ($R_m$ and $P_a$ given the same values for all simulations) to ease the comparison of the different step sizes used. The resulting rescaling of the time variable will then be determined by $\tilde{t} \approx 1.57 \cdot 10^{-3}\sqrt{\rho_\infty}$. The simulations giving the error as a function of the step size have been carried out with the airguns at the same depth thus the step sizes are directly comparable.

# 5 Results and discussion

In this section the KB-equation will be solved, and the test-equations (5.1) and (5.3) of which the exact solution is known ((5.2) and (5.4)) will be used to investigate the performance of the different methods described in section 3. The KB-equation will be used as a benchmark for the RFDE methods as well. The Matlab method dde23 and ddeConst with RFDE methods with coefficients given in section 4.1 as well as a fourth order CERK method has been applied.

## 5.1 Test-equation for RFDE methods

The first test equation

$$y'(t) = -y(t) + y(t-20) + \frac{t}{20}\cos\left(\frac{t}{20}\right) + \sin\left(\frac{t}{20}\right) \tag{5.1}$$

with exact solution

$$y(t) = \sin\left(\frac{t}{20}\right), \tag{5.2}$$

will be used to examine the order of the implemented methods without overlapping. The exact solution is $y \in \mathcal{C}^\infty$ and it is applied as the initial function, no breaking points will occur ($y'(t_0)^- = y'(t_0)^+$). As long as the step size $h \leq 20$ no overlapping will occur either, and the RFDE methods will behave as CRK-methods.

Solving the equation (5.1) without overlapping with ddeConst and the RFDE methods given in the tables (4.1),(4.2), (4.3), (4.4) and (4.5) as well as a fourth order CERK-method gave the error shown in figure 5.1. The error is given by $e = ||y(t_0+h) - y_{t_0+h}||_2$ where $y(t_0+h)$ is the exact solution at $t_0+h$ after one step starting at $t_0$ and $y_{t_0+h}$ is the corresponding solution achieved by using ddeConst with the method in question.

The methods clearly perform according to their order. The CERK-method is a little better than the fourth order RFDE methods. A reason for this might be the stronger restrictions on the coefficients of the RFDE methods giving less freedom for optimizing. To avoid problems with the machine precision, several intermediate calculations have been rounded off, and the methods maximum (reliable) accuracy for any step size $h$ is approximately $10^{-12}$.

Since the test problem has a long delay, investigation of the error when overlapping occurs is not natural, and a rewriting is necessary. The second

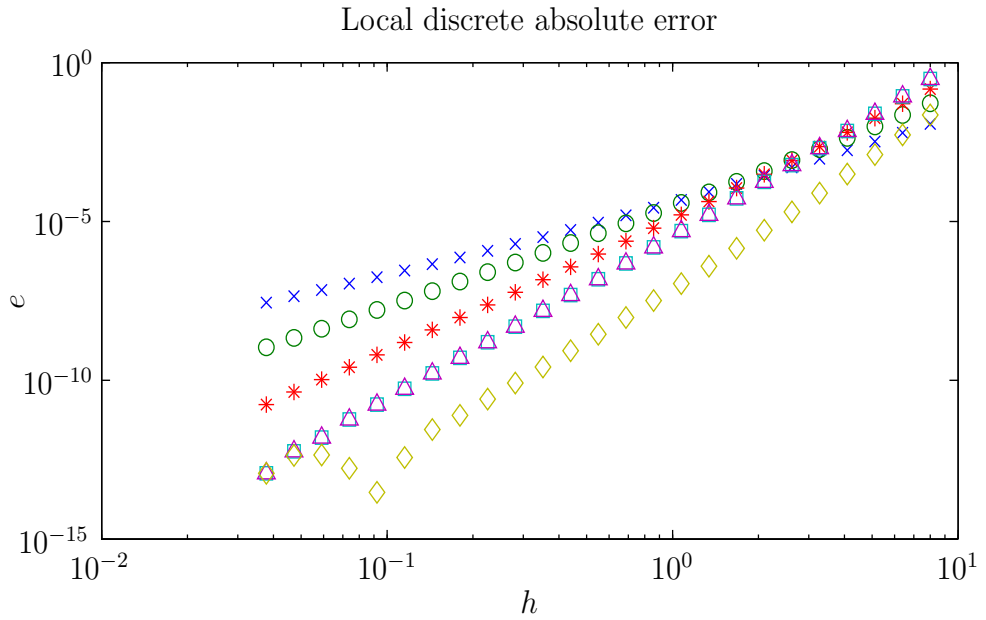


Figure 5.1: Local discrete absolute error from solving (5.1) with ddeConst and the methods given in tables (4.1) (×), (4.2) (○), (4.3) (∗), (4.4) (□), (4.5) (△) and a fourth order CERK method (◊).

test equation [1]:

$$y'(t) = -y(t) + y(t - 0.01) + 100t\cos(100t) + \sin(100t) \tag{5.3}$$

with exact solution

$$y(t) = \sin(100t). \tag{5.4}$$

will be used to examine the order with overlapping. The equation oscillates fast and a step size larger than $h = \frac{2\pi}{200} \approx 0.03$ is not reasonable because it may result in an accurate solution "by luck". The RFDE methods given in tables (4.2)-(4.5) have been applied and the errors are shown in figure 5.2. The methods behave as expected with exception of the second fourth order method (4.5) which seems to differ from the third order method (4.3) by a constant and not by $\mathcal{O}(h)$. The interval of interest is too narrow to draw any conclusions, so the methods are all at least assumed to be implemented correctly.

[1] It is difficult to find a good test-equation with known exact solution for investigating the error when overlapping occurs. The solution must vary enough when the delayed term alters, and still not vary to much all over. The equation used was by far the best suited of the ones explored.

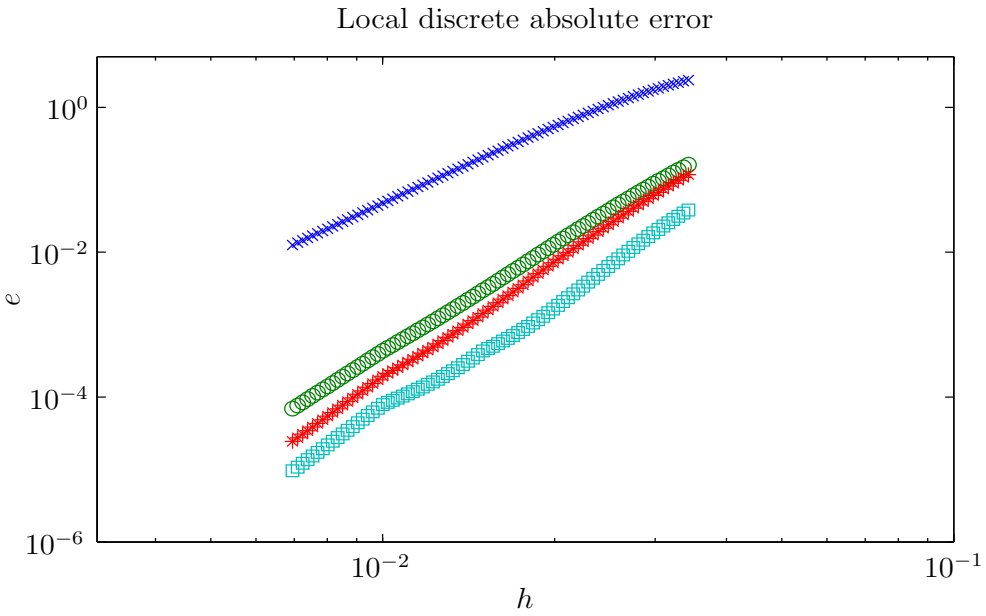


Figure 5.2: Local discrete absolute error from solving (5.3) with ddeConst and the methods given in tables (4.2) (×), (4.3) (∘), (4.4) (∗), (4.5) (□).

## 5.2 Kirkwood-Bethe equation

The KB-equation without including any delay arguments has been solved with ode45. When the delay arguments have been included, the equation has been solved with dde23 and ddeConst with the RFDE methods given in tables (4.1)-(4.5). The initial values for the different settings are given in table 5.1 and will be referred to by the given set number.

| | $V_0$ cm$^3$ | $T_0$ (K) | $P_0$ (bar) | $U_0$ (m/s) | $d$ (m) | $\frac{n_i}{n_{tot}}$ | $\tau$ (ms) | $\alpha$ | $\beta$ |
|---|---|---|---|---|---|---|---|---|---|
| set 1 | 655 | 290 | 140 | 0 | 7.5 | 1.0 | 0 | 0 | 0 |
| set 2 | 26 | 290 | 100 | 40 | 0.5 | 1.0 | 2 | 4.0 | 0.34 |
| set 3 | 26 | 290 | 100 | 40 | 0.5 | 0.8 | 2 | 6.7 | 0.48 |
| set 4 | 655 | 290 | 140 | 40 | 0.5 | 1.0 | 2 | 4.0 | 0.34 |

Table 5.1: Initial values used to solve the KB-equation.

### 5.2.1 General solution

The solution obtained without including any delayed terms and with initial data from set 1 is shown in figure 5.3. It has been integrated with ode45 with tolerances $AbsTOL = RelTOL = 10^{-6}$. The simulation corresponds to

the movement of the bubble produced by an airgun without any reflecting elements within a very large radius. The oscillation is damped and will die down after a certain time. The bubble period is approximately $t_B = 0.04$ s, and the movement of the bubble is close to identical the corresponding results obtained by Langhammer in [8].

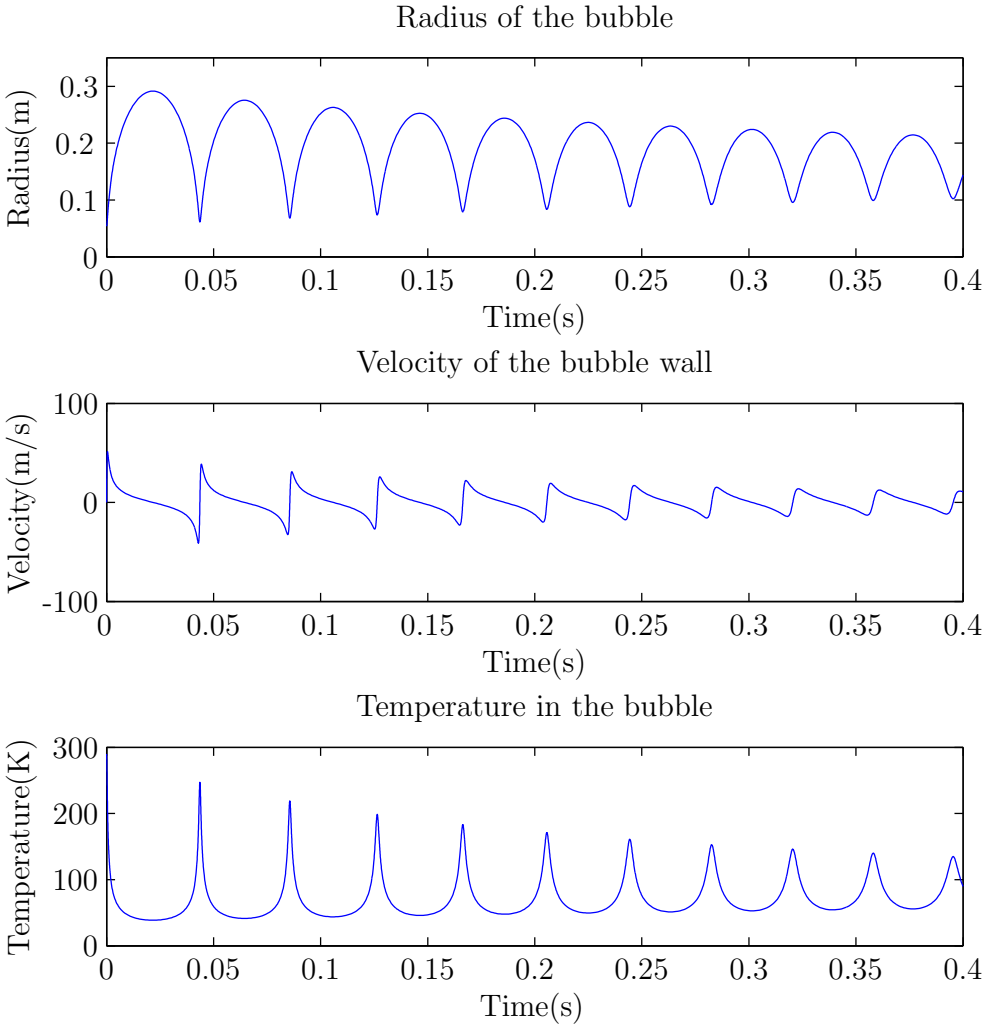


Figure 5.3: Solution of the KB-equation without delay arguments solved with ode45 and with initial data from set 1 in table 5.1.

When the ghost pressure is included, we need to use a DDE solver. Using ddeConst with the method given in table 4.4, step size $h = 10^{-4}$ and initial data from set 1 gave the results shown in figure 5.4. The period of the oscillation is prolonged slightly by the ghost pressure resulting in a bubble period of approximately $t_B = 0.041$ s. The amplitude is slightly larger than

the amplitude shown in figure 5.3 as well. The ghost pressure is inverted when it is reflected by the sea surface resulting in negative pressure peaks and positive pressure in between the peaks. A greater surrounding pressure would shorten the bubble period while a smaller pressure would prolong it. Hence the contribution from the peaks are the most significant. The reflection coefficient has been set to $\gamma = -1$.

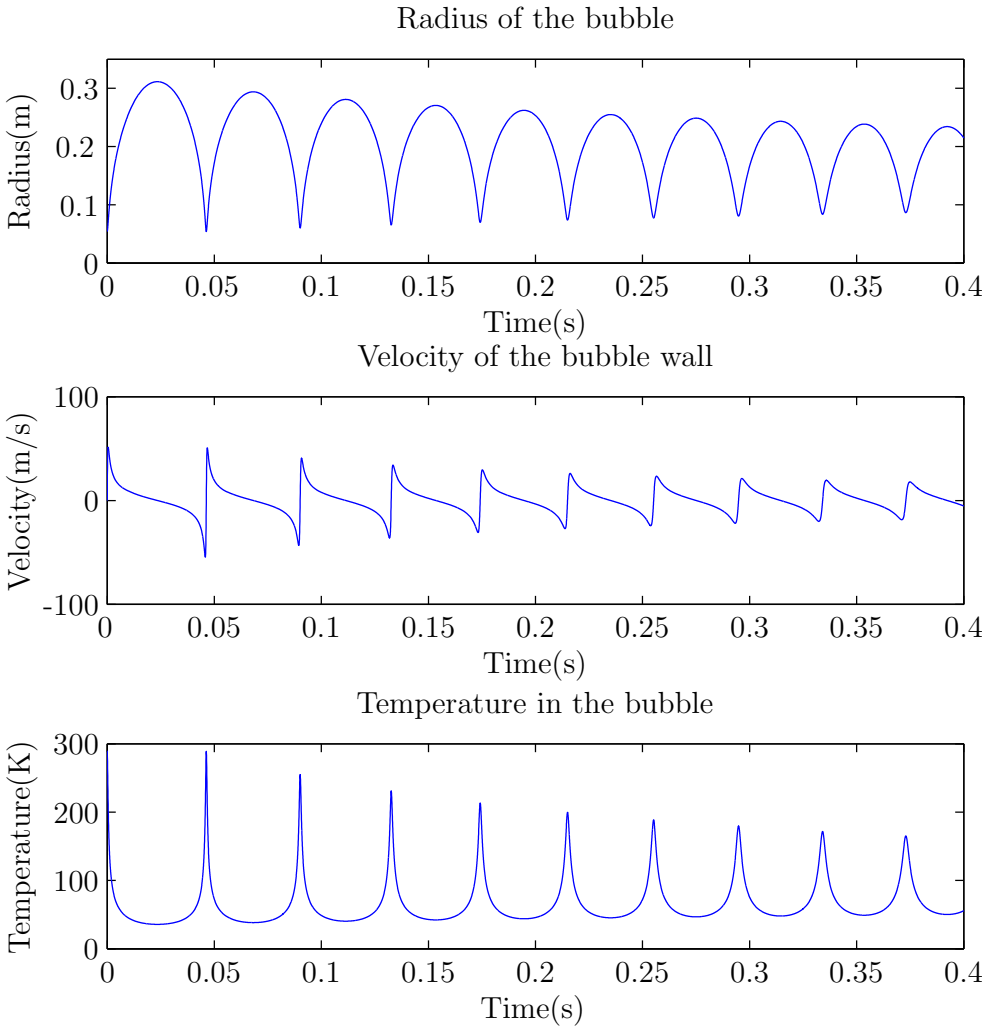


Figure 5.4: Solution of the KB-equation solved with ddeConst, the method given in table (4.4) and step size $h = 10^{-4}$ (no overlapping). Ghost pressure is included and initial data from set 1 in table 5.1 have been used.

When the pressure wave hits the bubble, it does not cause any sudden changes in the movement of the bubble. The change in hydrostatic pressure is included in the equations (2.17) only through the expression $p(\infty) + B$ where

$B = 3000$ atm thus the pressure wave represents a relatively small change. Also the entalpi (given in (2.17d)) where it is not that easy to discover the consequences of a change in the hydrostatic pressure do seem to react little to the pressure changes. Originally the presence of the hydrostatic pressure in the equations arise from the change in density and the according change of the sound velocity given by the Tait equation (2.11). The changes in the sound velocity and density of water due to pressure influence is small, so even for very large pressure changes they vary little.

The common integrators used today have shown problems when simulating large airguns close to the surface. The reflected pressure wave may then give a negative total pressure around the airgun bubble. The solution will not be physically correct, and the simulation breaks down. This problem has not been recreated. Even a two-gun simulation where one airgun had initial pressure of $P_0 = 3400$ bar and chamber volume of $V_0 = 655$ cm$^3$ at $d = 1$ m depth resulting in a negative pressure of $p_{del} = 20$ bar around the neighboring airgun made the simulation break down.

### 5.2.2 Pressure signatures

The pressure signatures from a single airgun have been well studied and tested. For every type of airgun, testing is needed to determine simulation constants that are unique for every airgun type. The testing is normally carried out in a deep fjord where the water is still and where it is deep enough to avoid unwanted interference from the sea bottom reflections.

As a reference signature the results provided by Langhammer in [8] have been used, mainly because the simulation coefficients used to simulate a copy of the recorded signature is given in the paper. The measured signature is shown together with Langhammer's simulation in figure 5.5.

Solving the KB-equation with ddeConst, the RFDE method given in table 4.4 and the initial values given in set 2 resulted in the pressure signature in figure 5.6. The ddeConst signal is sharper and the bubble period is shorter than in figure 5.5 and although the amplitudes are similar, the difference is too big to be neglected. In addition Langhammer comments on how the initial transfer process of gas from the chamber into the water had a great influence on the pressure signal ($n_i$ and $\tau$ are not given) while the signal in figure 5.6 has been modeled with $n_i = n_{tot}$. Any initial gas injection process would result in a smaller bubble radius and a smaller bubble period. If the injection process is used together with altered empirical coefficients $\alpha$ and $\beta$, the results closest to the one given in figure 5.5 were achieved by initial data given in set 3, still only reproducing a result very similar to the result shown in figure 5.6. The bubble radius and bubble wall velocity from the simulation

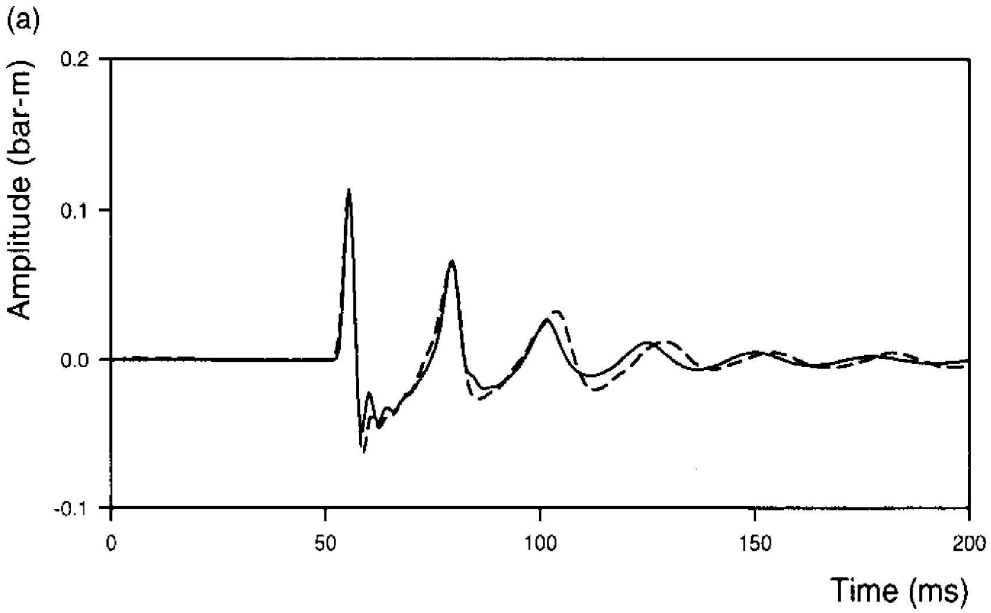


Figure 5.5: Modeled signature from solving the KB-equation with $\alpha = 4$ and $\beta = 0.34$ (solid line) and measure pressure signature from a BOLT 600B airgun with initial volume of 26 $cm^3$ and initial pressure of 100 bar (dashed).

with initial data from set 2 were a lot closer to Langhammer's simulation, and this comparison did not reveal the difference in the bubble period that clearly as the bubble radius oscillation die out too fast.

The simulation with initial data from set 2 will be used and the difference from any "more correct" solution should not affect the validity of this equation as a benchmark for the RFDE methods. The dde23 method gave similar results to ddeConst with method given in table 4.4 for all initial data sets, thus the difference lies in the implementation of the equations and/or the filter. This simulation will also be used to investigate the effect of pressure waves of different magnitudes on the motion of the airgun bubble and its corresponding output pressure wave. Again we assume the obtained solutions to be "good enough".

### 5.2.3 Two-gun cluster

In seismic surveys today it is common to construct airgun clusters consisting of two airguns. The interaction between the airguns must be included in the physical model describing the motion of the airgun bubbles. The airguns are normally placed at the same depth and rather close to each other (1-2 m). If the bubbles are too close, nonlinear effects affect the interaction between the

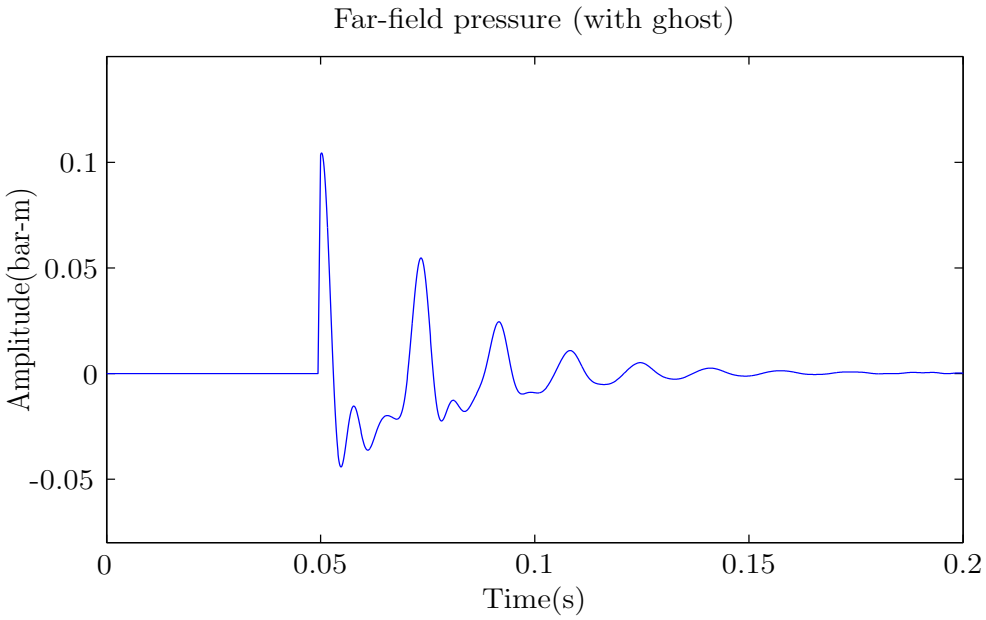


Figure 5.6: Far-field pressure obtained by solving the KB-equation with ddeConst, the method given in table 4.4 and step size $h = 10^{-4}$. Ghost pressure has been included and initial data from set 2 in table 5.1 have been used.

bubbles and must be taken into account. This critical distance is normally exceeded to avoid nonlinear effects.

Both the direct pressure and the ghost pressure from the neighboring airgun are included in the simulation. The joint output pressure waveform in the far-field from two airguns with the initial data from set 2 is shown in figure 5.7. The pressure signature has as expected about twice the amplitude of the signature from one airgun. Other than this, the signature resembles a lot the signature shown in figure 5.6. If the interaction between the two guns as well as the reflection from the sea surface is omitted, the resulting signature would be the one shown in figure 5.8.

The difference from figure 5.7 is small but clear, thus the delayed interaction between the airguns affects the pressure signature and must be included if recreation of a measured pressure signature is to be obtained.

If the cluster consists of airguns of different sizes, the pressure wave from the larger airgun will probably make a bigger impact on the smaller airgun than in the previous cases. The sole far-field pressure signature from the smaller airgun (initial data from set 2) when deployed near a larger airgun (initial data from set 4) is shown in figure 5.9.

When the smaller airgun is under influence from the larger airgun, the signature has a slightly smaller amplitude but approximately the same bubble

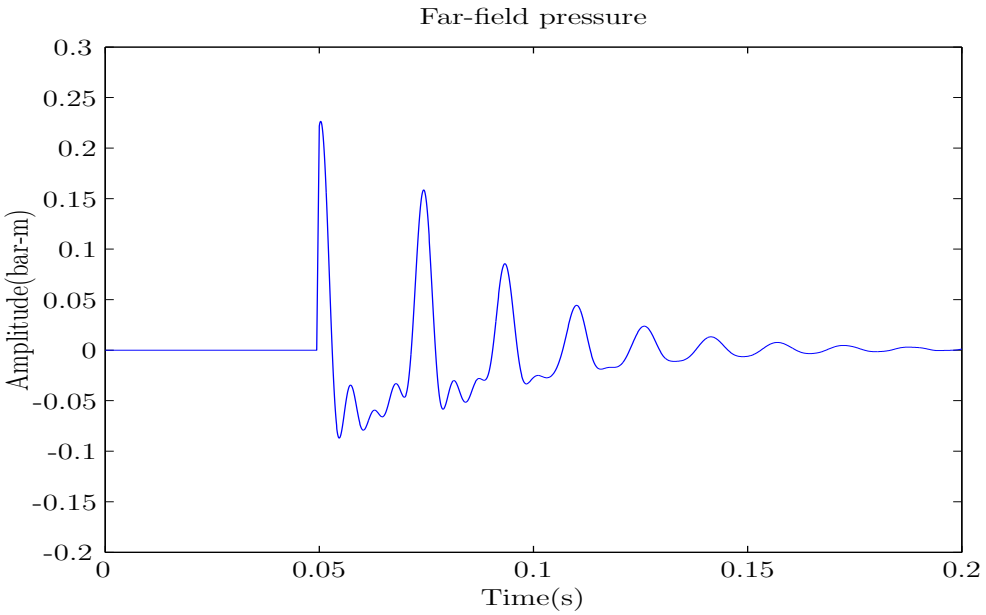


Figure 5.7: Far-field pressure obtained by solving the KB-equation with dde-Const, the method given in table 4.4 and step size $h = 10^{-4}$. Delayed pressure has been included, initial data from set 2 in table 5.1 have been used and the distance between the airguns has been set to 1 m.

period as the signature from the smaller airgun alone (in figure 5.6). In addition the smaller airgun's amplitude seems to be less damped, or in other words the larger airguns pressure wave contribute against the dampening of the smaller airguns bubble. This is though only a marginal effect. The general result is in agreement with the opposite effect from the ghost pressure.

The need for explicit methods that stay explicit in the case of overlapping can be illuminated by looking at the maximum step size dde23 uses when solving the KB-equation for two airguns with initial data from set 2 integrated over the interval $t \in [0, 0.1]$. The absolute and relative tolerances have been varied. The maximum step sizes are given by means of the dimensionless variable $\hat{t}$ with the delays $\hat{\tau_1} = \hat{\tau_2} = 0.01342$ and $\hat{\tau_2} = 0.01898$. The results are shown in table 5.2.

The standard values for the relative and absolute tolerances are $10^{-3}$ and $10^{-6}$ respectively. With these settings, the maximum step size does exceed the smallest delay. Other likely combinations of the two tolerances also gives this result. For very large tolerance bounds (causing overlapping in a large amount of steps) dde23 used a lot more time to integrate over the given interval assumingly because of the additional computational costs related to the iteration used when calculating the overlapping delay values. Hence, it

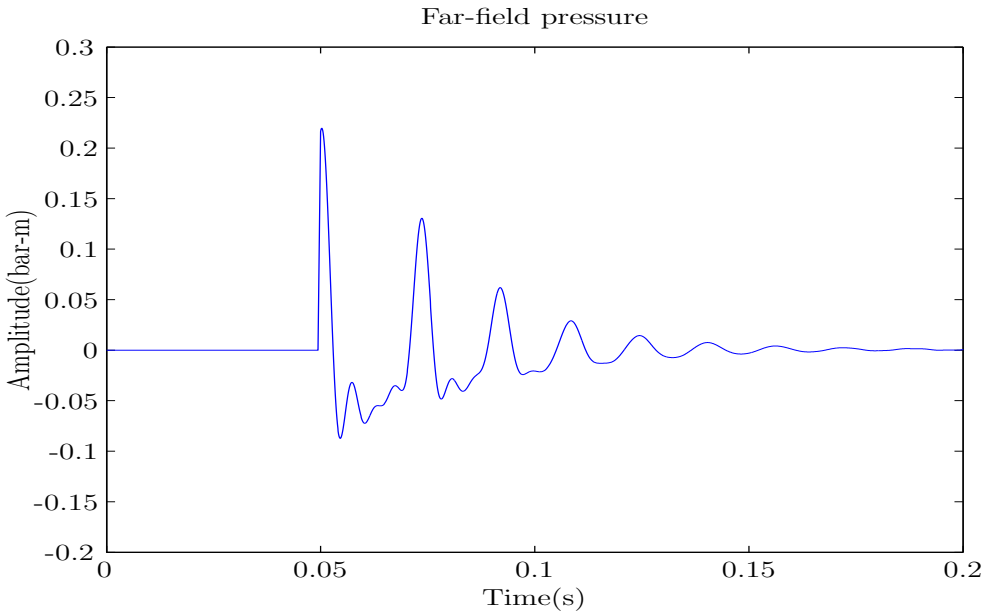


Figure 5.8: Solution of the KB-equation solved ddeConst, the method given in table 4.4 and step size $h = 10^{-4}$. All delayed pressure is omitted, initial data from set 2 in table 5.1 have been used and the distance between the airguns has been set to 1 m.

is reasonable to investigate the use of RFDE methods that stay explicit in the case of overlapping and use these to solve the KB-equation.

### 5.2.4 RFDE method performance

The solution of the KB-equation and the influence of different outer pressure waves have been shown in the previous section. The solution obtained with ddeConst with the methods given in table 4.4 without overlapping has mainly been used. The remaining methods will here be applied to investigate their performance on the KB-equation compared with the solution obtained by dde23 with tolerance $AbsTOL = RelTOL = 10^{-10}$. The calculated error $e$ is the local discrete absolute error when solving the KB-equation for two coupled airguns with initial data from set 2 in table 5.1 with distance 1 m between the airguns and integrated one step. The error is given by $e = ||y(t_0 + h) - y_{t_0+h}||_2$ where $y(t_0 + h)$ is the solution from dde23 and $y_{t_0+h}$ is the solution obtained with ddeConst. As an illustration of the magnitude of the errors, the solution of ddeConst with the method given in table 4.4 with a step size of $h = 0.0075$ has been plotted together with the solution obtained with dde23 in figure 5.10. The error in the first step is here $e = 1.223$ and

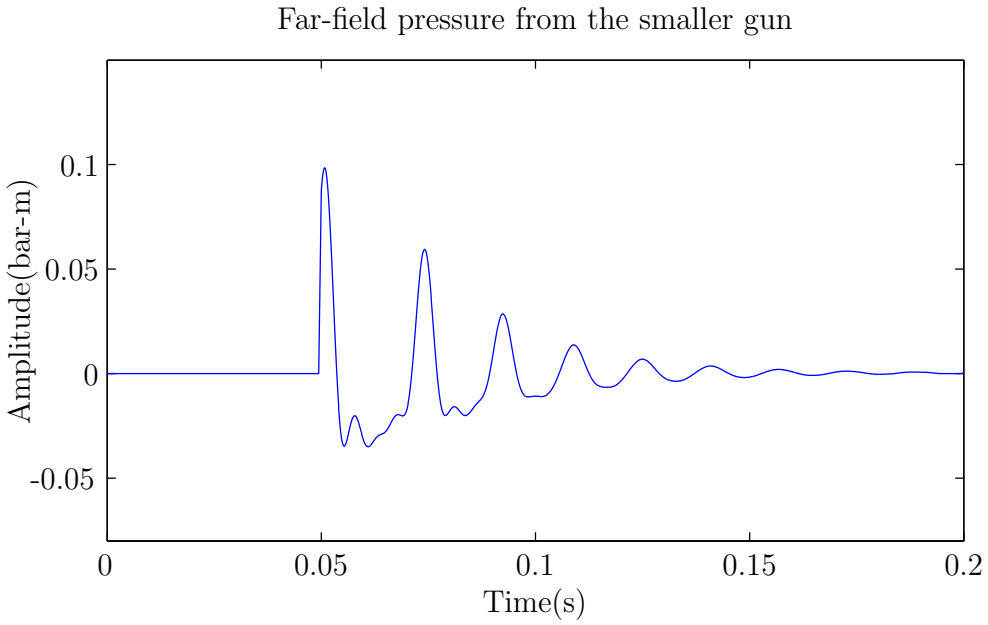


Figure 5.9: Far-field signature from the smaller airgun obtained by solving the KB-equation with ddeConst, the method given in table 4.4 and step size $h = 10^{-4}$. Two airguns of different sizes with initial data from respectively set 2 and set 4 in table 5.1 with a distance between the guns of 1 m have been simulated.

the solution seems to develop in a similar way in all variables compared to the solution obtained with dde23.

The resulting errors for all RFDE methods are shown in figure 5.11. The behavior of the last four methods is somewhat strange. The deviation from the expected straight line may origin from the large change in variables at the start of the integration and/or the stiffness of the equations in the initial phase[2]. A thorough analytic study of the RFDE methods' behavior when applied to the KB-equation lies outside the scope of this thesis, and we belive that the methods performs within a satisfying range of the expected order. In addition it seems that an error smaller than $10^{-6}$ is not possible to achieve. This may be caused by rounding off intermediate calculations which contribute to a larger error when solving the KB-equation than solving the test equation (5.1). If so, this inaccuracy would most likely also be the source for some of the strange behavior seen in figure 5.11. As a result of this the global error control given by (3.12) would, if implemented into the

[2]In my project work I found that the equations are stiff in the initial phase. This result was obtained by calculating the eigenvalues of the Jacobian and analyzing step lengths and corresponding errors.

| Rel\Abs | $10^{-3}$ | $10^{-4}$ | $10^{-5}$ | $10^{-6}$ | $10^{-7}$ | $10^{-8}$ |
|---|---|---|---|---|---|---|
| $10^{-3}$ | **0.04863** | **0.03194** | **0.03194** | **0.03194** | **0.03194** | **0.03194** |
| $10^{-4}$ | **0.04862** | **0.02785** | 0.01342 | 0.01342 | 0.01342 | 0.01342 |
| $10^{-5}$ | **0.04862** | **0.02770** | 0.01342 | 0.00972 | 0.00706 | 0.00666 |
| $10^{-6}$ | **0.04862** | **0.02770** | 0.01342 | 0.00754 | 0.00439 | 0.00322 |
| $10^{-7}$ | **0.04862** | **0.02770** | 0.01342 | 0.00744 | 0.00354 | 0.00207 |
| $10^{-8}$ | **0.04862** | **0.02770** | 0.01342 | 0.00744 | 0.00353 | 0.00166 |

Table 5.2: Maximum step size when integrating the KB-equation for two airguns with initial data given in set 2 over the interval $t \in [0, 0.1]$. The step size is given in the dimensionless variable $\hat{t}$. The step sizes that exceed the smallest delay are written in bold face. Rel\Abs is the relative local error and the absolute local error respectively.

ddeConst solver, not provide any step size satisfying an absolute error bound smaller than approximately $10^{-3}$ even with the fourth order methods. This is a serious limitation and does indeed make the use of RFDE methods less interesting. To their defence it can be said that integrating the KB-equation in its initial phase is indeed a difficult task.

The rescaling of the time variable results in the three delays $\hat{\tau_1} = \hat{\tau_2} = 0.01342$ and $\hat{\tau_2} = 0.01898$ hence no overlapping occurs with the step sizes used in figure 5.11. Further integration with step sizes close to the delays with any of the methods led to diverging solutions. The investigation of the errors with overlapping has therefore been carried out with $t_0 > \max_i \tau_i$ and with the dde23 solution as the initial function. This has two important consequences. First, the solution changes slower and can be integrated with a larger step size (assuming no limiting stiffness in the equation for $t > t_0$), and second the initial value satisfies the equation thus no breaking points occur. With $\hat{t_0} = 0.5$ the local discrete absolute errors for the RFDE methods given in tables 4.2-4.5 are shown in figure 5.12.

Here another surprise is revealed. The third order method performs equal to the second order method. The comparison of the second order method with the two fourth order methods give expected results, and the error is over all smaller than for the integration with $t_0 = 0$. Again this result was not detected when integrating the test equation (5.3) and it is hard to pinpoint the origin of this effect without a thorough analytic study.

### 5.2.5 Linear interpolation

To investigate the need for a high order dense representation of the solution, the interpolation technique has been changed to linear interpolation for all

methods. In section 5.2.2 we saw that the outer pressure influence on the bubble was small thus it is not a great surprise when the difference between the solution with high order interpolation and linear interpolation was practically zero for all methods and all step sizes. Meaning that the difference was smaller than the accuracy of the method $e < 10^{-12}$. The difference in the delayed values collected from the stored values was $< 10^{-2}$ and the difference in the delayed pressure calculated from these even smaller.

In addition an even less accurate interpolation was applied: a constant interpolation where the value at the closest nodal point was used. The overlapping technique was changed to the constant version by using the values from the latest nodal point (constant extrapolation). The difference between the method with the regular interpolation technique and the method with the constant interpolation technique was also non-detectable.

### 5.2.6 Diverging solutions

Further integration of the KB-equation from $\hat{t} = 0.5$ with the Heun method (4.2) did, as all methods with large step sizes when $\hat{t} = 0$ did, diverge for the largest step sizes used in figure 5.12. The diverging solutions are easy to explain. In the initial face the bubble expands fast (also at $\hat{t} = 0.5$ though a lot slower than at $\hat{t} = 0$) and the rapid change in all variables result in an unstable integrator when the step size is too large. If the inaccurate numerical solution approximates a too large bubble after one step, the forces compressing the bubble will be very strong and result in a too small bubble after the next step. The following step will give an even larger bubble than the first one. The amplitude of this oscillation will grow very large.

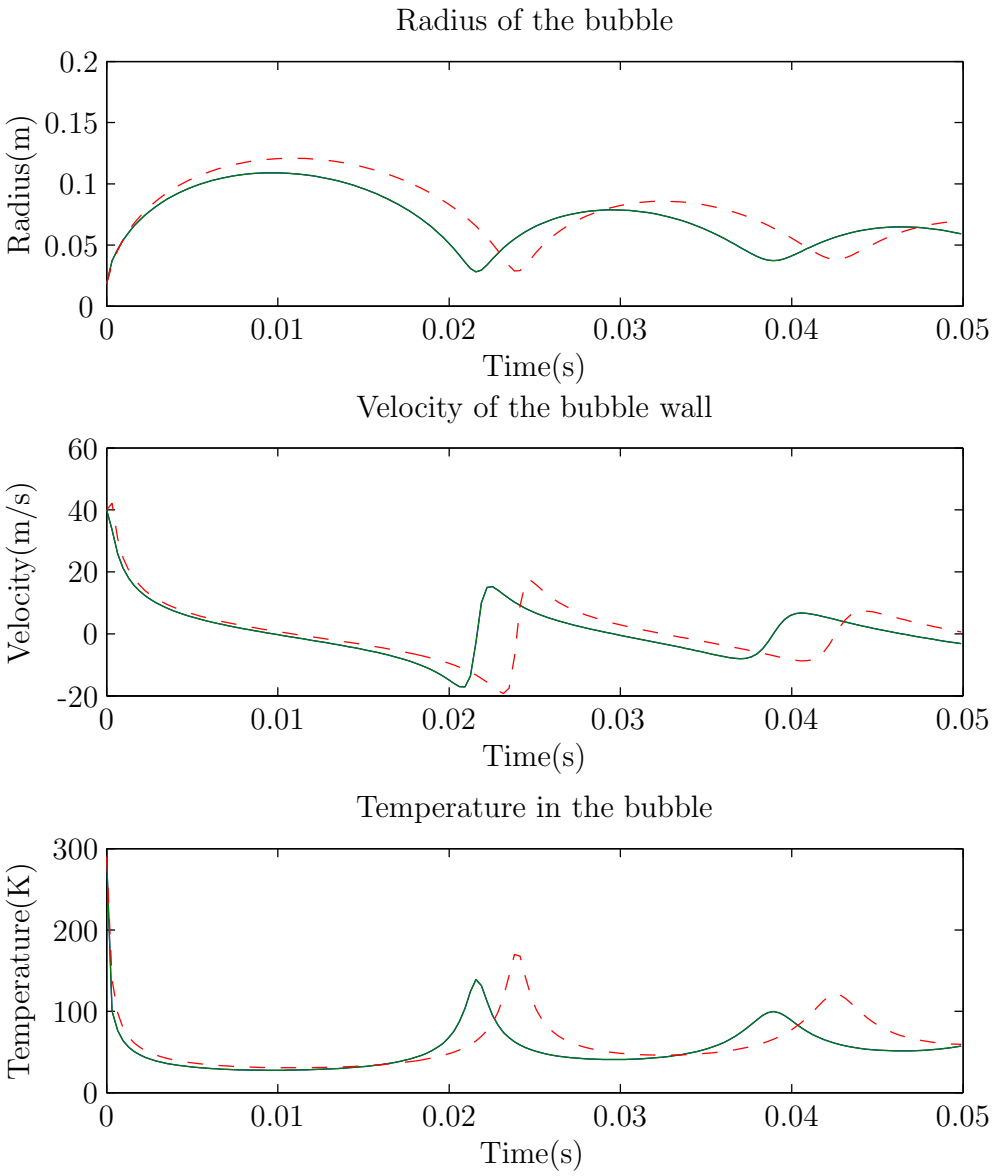


Figure 5.10: Solution of the KB-equation solved with ddeConst, the method given in table 4.4, step size $h = 10^{-4}$ and initial data from set 2 in table 5.1 (solid line) along with the solution from solving the same equation with dde23 with the tolerance values $AbsTOL = RelTOL = 10^{-10}$ (dashed).

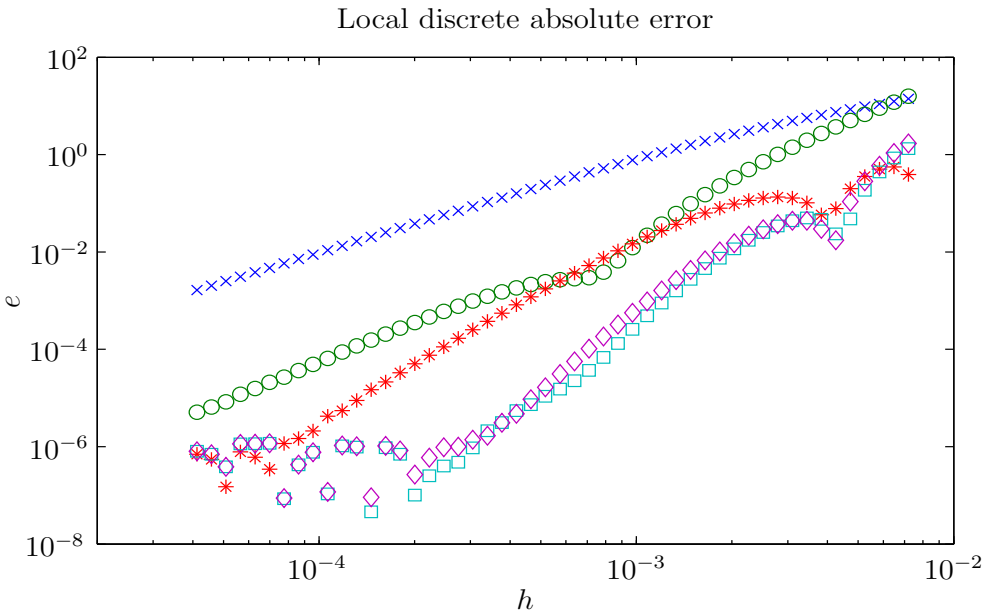


Figure 5.11: Local discrete absolute error for the solution of two coupled KB-equations solved with ddeConst with RFDE methods given in table (4.1) ($\times$), (4.2) ($\circ$), (4.3) ($*$), (4.4) ($\square$) and (4.5) (*Diamond*) with $\hat{t_0} = 0$.

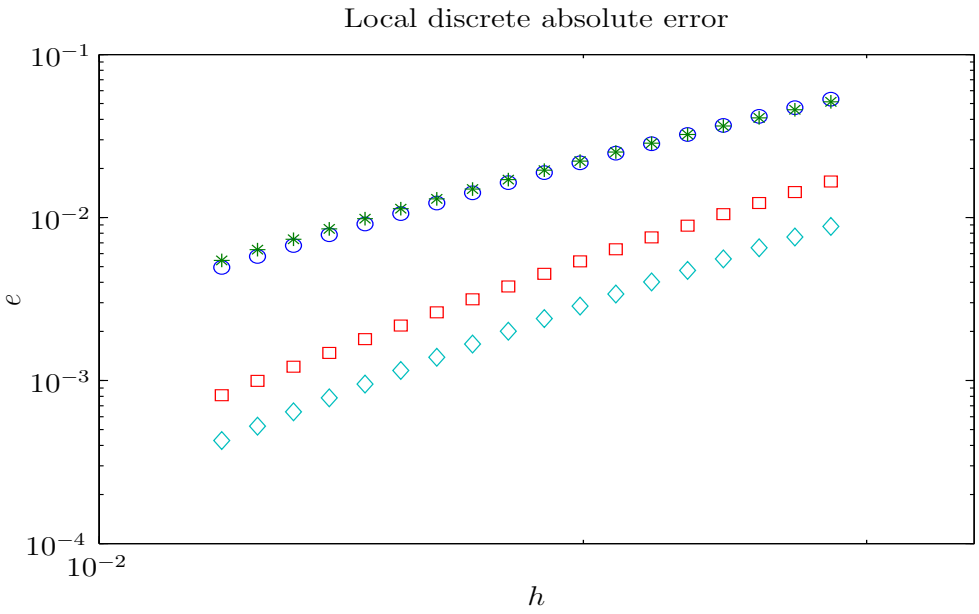


Figure 5.12: Local discrete absolute error for the solution of two coupled KB-equations solved with ddeConst with RFDE methods given in table (4.2) ($\circ$), (4.3) ($*$), (4.4) ($\square$) and (4.5) (*Diamond*) with $\hat{t_0} = 0.5$.

# 6 Conclusion

The KB-equation has been solved with several methods and the performance of these methods, both with and without overlapping has been investigated. The main areas of interest are simulation the pressure signature from an airgun and how RFDE methods of different orders performs when solving the airgun equations.

## 6.1 Pressure waves

It is a manageable task to recreate the transmitted signal from airguns in simulations. Although several empirical parameters which varies for different airgun types, and even different filters (each oil company seem to use different filters) are used to obtain the simulated signal. Hence not all physical aspects of the motion of an airgun bubble and of the pressure wave propagation are known.

The resulting output pressure wave from the simulations described in this thesis match other corresponding results only to a certain point. As a consequence the results derived from pressure signatures are mainly interpreted as qualitative. The difference between two pressure signatures obtained from the equations with variating influence from outer conditions are assumed to represent the difference we would get from the same influence variation with a "more correct" simulated pressure signature.

When two airguns are combined in a cluster, their pressure signatures have shown a small but clear effect on the neighboring airgun's behavior. The pressure reflected from the sea surface also showed an influence on the bubble. Normally the airguns are placed at a depth where this effect diminishes, and the change in the hydrostatic pressure due to the ghost pressure is very small. Still it is not possible to determine quantitatively from the data presented here whether it is an option to neglect this pressure or not. It is clear that the ghost pressures effect on the joint pressure wave in the far-field is significant and must be included and that the effect of the direct pressure propagating from one airgun to the other is too big to be neglected.

## 6.2 RFDE methods

Together with the implemented DDE solver ddeConst, the RFDE methods given in tables 4.1-4.5 were used to solve the two test equations (5.1) and (5.3) as well as the KB-equation (2.17).

When dde23 was used to solve the KB-equation with somewhat large though reasonable tolerance bounds, its largest step size was larger than

the smallest delay. When this overlapping occurred, the computational costs involved in calculating the delay values were relatively high. Hence, it seemed possible to improve the efficiency of the integrator by use of methods that handles overlapping better: RFDE methods.

The results obtained when applying the RFDE methods to the test equations showed that although the methods handled overlapping well, the fourth order RFDE methods were in general less efficient than the fourth order CERK method. When the RFDE methods were applied to the KB-equation, this lack of general efficiency resulted in an unsatisfying performance. So, although the methods does stay explicit in the case of overlapping, the overall accuracy leads to shorter step sizes than the smallest delay even with high tolerance bounds.

The accuracy of the continuous extension of the solution had very little impact on the general error. Even when a constant interpolation technique replaced the regular dense solution in the fourth order RFDE methods, the difference in the obtained solution was impossible to detect.

All together it seems that the RFDE methods, the implementation of them and/or the conditioning of the KB-equation must be improved significantly. Otherwise the best integrator for the KB-equation would be a standard CERK method or an ERK method with additional interpolation. The effect of an unaccuracy in the calculated delay values is so small that a linear interpolation will provide a good enough solution.

The RFDE methods showed high accuracy when applied to the test equations and may be valuable when other problems concerning interacting bodies with delays are to be solved. For the KB-equation however they have proven dispensable. Both due to the insensitivity with respect to the accuracy of the delay values and the marginal need of step sizes that result in overlapping.

## 6.3 Airgun arrays

The ability to efficiently simulate the joint output pressure wave from an airgun array has not been significantly improved by use of any of the methods explored in this thesis. The most interesting result in this context would be the needlessness of accurate interpolation techniques which may be exploited to better the efficiency of the numerical solvers to a certain extent. Nevertheless it has been shown that overlapping will occur when using an accurate high order method, hence the need of methods that stay explicit in those cases will prove useful if their general accuracy is good enough.

# 7 Further work

The RFDE methods proved bad suited for solving the KB-equation. Both improving the RFDE methods as well as exploring other methods for solving the KB-equation are interesting tasks. The airgun equations themselves may also be analyzed to better the conditioning of the system. The KB-equations may also be extended to include further physical effects.

## 7.1 Numerical methods

The RFDE methods and the implementation of them are possible to improve. Especially the implementation which has not been thoroughly studied and where the errors which origin from the machine error has not been determined. It may also be an interesting task to analyze the calculations carried out when solving the KB-equation to construct a customized solver.

An interesting potential for improvement lies in the fact that bodies which only interact through delayed terms result in a system of equations where the k'th subsystem only depends on the other subsystems through the delayed terms. A more thorough study of the RFDE methods or other similar methods can be carried out to exploit this fact. Hopefully resulting in more accurate methods where larger step sizes can be used and the overlapping technique in the RFDE methods will be well suited.

## 7.2 Airgun simulation

There exists better simulators that obtain the output pressure wave from an airgun cluster than the one implemented in this thesis, where many hydrodynamical aspects have been overlooked. When two interacting airguns are placed very close to each other or very close to the surface, the linear pressure interaction model must be extended to include nonlinear terms as well. When an accurate simulator of a two gun cluster is implemented, it can be extended to simulate more than two guns. If non-linear terms must be taken into account, this could prove an interesting task.

The joint pressure output wave from several clusters can be optimized with respect to the combination of airgun sizes as well as the firing timing. Here lies many mathematical problems to explore.

# References


[1] Energy Information Administration. World consumption of primary energy by energy type and selected contries. Homepage of Energy Information Administration, July 2006. http://www.eia.doe.gov/emeu/international/energyconsumption.html, downloaded: 06.27.07.

[2] Alfredo Bellen and Marino Zennaro. *Numerical methods for delay differential equations*. Numerical Mathematics and Scientific Computation. The Clarendon Press Oxford University Press, New York, 2003.

[3] Jon F Claerbout. *Fundamentals of Geophysical Data Processing*. Blackwell Scientific Publications, 1985.

[4] Colin W. Cryer and Lucio Tavernini. The numerical solution of Volterra functional differential equations by Euler's method. *SIAM J. Numer. Anal.*, 9:105–129, 1972.

[5] Ernst Hairer, Syvert P. Nørsett, and Gerhard Wanner. *Solving ordinary differential equations. I*, volume 8 of *Springer Series in Computational Mathematics*. Springer-Verlag, Berlin, second edition, 1993. Nonstiff problems.

[6] Sam Howison. *Practical applied mathematics*. Cambridge Texts in Applied Mathematics. Cambridge University Press, Cambridge, 2005. Modelling, analysis, approximation.

[7] John G Kirkwood and Hans A Bethe. Shock and detonation waves. In *John Gamble Kirkwood collected works*. Gordon and Breach, 1942.

[8] Jan Langhammer. *Experimental studies of energy loss mechanisms in airgun bubble dynamics*. PhD thesis, NTH (now NTNU), 1994.

[9] Stefano Maset, Lucio Torelli, and Rossana Vermiglio. Runge-Kutta methods for retarded functional differential equations. *Math. Models Methods Appl. Sci.*, 15(8):1203–1251, 2005.

[10] Robert E Sheriff and Lloyd P Geldart. *Exploration Seismology*. Cambridge University Press, 1995.

[11] Anton Ziolkowski. A method for calculating the output pressure waveform from an air gun. *Geophysical Journal of the Royal Astronomical Society*, 21:137–161, 1970.

# A Appendix

## A.1 Rayleigh equation

Rayleigh derived the equation describing the movement of the bubble wall for a gas filled cavity in 1917. His theory will be presented here. Let us for now forget about the actual airgun and consider only an oscillating air bubble in water. The simplest way to describe the movement of the air bubble is to consider a cavity filled with gas in an incompressible liquid of infinite extent.

### A.1.1 Model

We assume spherical symmetry and write the kinetic energy $e_k$ of a spherical shell in the liquid of infinitesimal thickness $\mathrm{d}r$ and mass $m$ as

$$e_k = \frac{1}{2}mu^2 = \frac{1}{2}\rho 4\pi r^2 \cdot \mathrm{d}r \cdot u^2, \tag{A.1}$$

where $u$ is the velocity, $\rho$ is the density and $r$ is the distance to the center of the bubble. The radius of the bubble $R$ and the velocity of the bubble wall $U$ will, due to the incompressibility and hence continuity of mass, fulfill

$$u = U\left(\frac{R}{r}\right)^2. \tag{A.2}$$

With equation (A.2) inserted in (A.1) and integrated from $R$ to $\infty$, the total kinetic energy $E_k$ of the liquid can be described by the variables at the bubble wall

$$E_k = \frac{1}{2}\rho 4\pi \int_R^\infty \left(U\left(\frac{R}{r}\right)^2\right)^2 r^2\,\mathrm{d}r = 2\rho\pi U^2 R^4 \int_R^\infty \frac{1}{r^2}\,\mathrm{d}r = 2\rho\pi U^2 R^3.$$

If there is no heat transfer between the bubble and the liquid, all change in the liquids kinetic energy must be caused by work $W$ done by the bubble on the liquid,

$$W = -(p(R) - p(\infty))\frac{4}{3}\pi R^3,$$

where $p(R)$ is the pressure in the bubble and $p(\infty)$ is the hydrostatic pressure at the same depth as the bubble. Then

$$\frac{\mathrm{d}}{\mathrm{d}t}(E_k + W) = 0 \;\Rightarrow\; 2\rho\pi\left(2UR^3\dot{U} + 3U^2R^2\dot{R}\right) = (p(R) - p(\infty))4\pi R^2\dot{R}, \tag{A.3}$$

where $\dot{R} = \frac{\mathrm{d}}{\mathrm{d}t}R = U$ and $\dot{U} = \ddot{R}$. The next assumption is that the gas obeys the ideal gas law $pV = nR_gT$ where $p$ is the pressure, $V$ is the volume, $n$ is mol gas, $R_g$ is the ideal mol gas constant and $T$ is the temperature. Then

$$\mathrm{d}Q = \mathrm{d}E_u + p\mathrm{d}V, \tag{A.4}$$

where $Q$ is heat energy and $E_u$ is inner energy. By using $(\partial_T E_u)_{V,n} = c_V n$ where $c_V$ is the heat capacity per mol with constant volume, and assume that $c_V$ is independent of the temperature $T$, $E_u = c_V nT + k$ where $k$ is a constant. Then $\dot{E}_u = c_V(\dot{n}T + n\dot{T})$ and no mass transfer between the bubble and the liquid, $\dot{n} = 0$, makes the following rewriting of (A.4) possible:

$$\dot{T} = -\frac{p\dot{V}}{c_V n}. \tag{A.5}$$

Equation (A.5) and equation (A.3) gives the full description of the movement of the bubble:

$$\dot{R} = U, \tag{A.6a}$$

$$\dot{T} = -\frac{p\dot{V}}{c_V n}, \quad \dot{V} = 4\pi R^2 \dot{R}, \tag{A.6b}$$

$$\dot{U} = \frac{p(R) - p(\infty)}{\rho R} - \frac{3}{2}U^2, \quad p(R) = \frac{3nR_gT}{4\pi R^3}. \tag{A.6c}$$

This model is rather coarse and not suitable either for describing the actual movement of the bubble created by an airgun, or for simulating the output pressure waveform, but it is easy to understand and can serve as a "dummy" for the Kirkwood-Bethe (KB) model.

### A.1.2 Dimensionless form

We want to rewrite equation (A.6) to be solely expressed by dimensionless variables. This will improve the conditioning of the system. Let

$$R \;\rightarrow\; R_m y_1, \quad U \;\rightarrow\; U_m y_3, \quad T \;\rightarrow\; T_0 y_2,$$

where $R_m$ is the maximal bubble radius, $U_m$ is the maximal velocity of the bubble wall and $T_0$ is the initial temperature. The equations become

$$\dot{y_1} = y_3, \tag{A.7a}$$

$$\dot{y_2} = -\frac{pR_m^3}{c_V nT_0} y_1^2 y_3, \tag{A.7b}$$

$$\dot{y_3} = \frac{3T_0 nR_g}{4\pi U_m^2 R_m^3 \rho}\frac{y_2}{y_1^4} - \frac{p(\infty)}{U_m^2 \rho}\frac{1}{y_1} - \frac{3R_m}{2}y_3^2, \tag{A.7c}$$

which can be solved numerically with initial values $y_1 = R_0$, $y_2 = T_0$ and $y_3 = 0$.

The Rayleigh equation (A.7) solved with ode45 and with initial values $V_0 = 655$ cm$^3$, $T_0 = 290$ K, $P_0 = 140$ bar and $d = 7.5$ m.

From figure A.1.2 we see that the energy of the system is preserved and the oscillation will continue forever. The Rayleigh equation is easy to understand, and the basic physics invloved in an airgun blast is illustrated. The KB-equation is generally only including additional hydronamical effects.

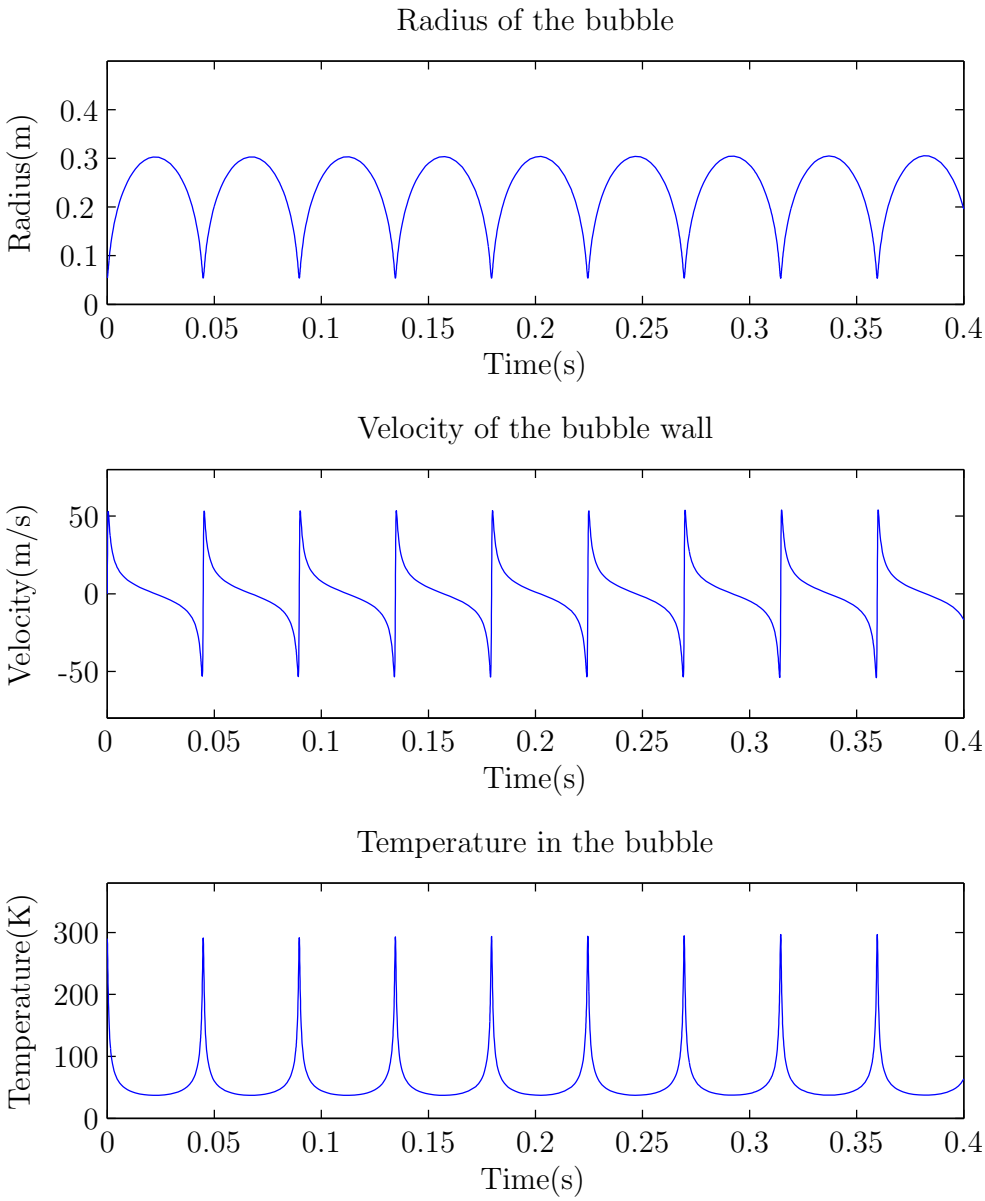


Figure A.1: Solution of the Rayleigh equation solved with ode45.